

MODIS–Landsat fusion for large area 30 m burned area mapping

Luigi Boschetti ^a, David P. Roy ^b, Christopher O. Justice ^c, Michael L. Humber ^c

^a Department of Forest, Rangeland and Fire Sciences, University of Idaho, Moscow, ID 83843, United States

^b Geospatial Sciences Center of Excellence, South Dakota State University, Brookings, SD 57007, United States

^c Department of Geographical Sciences, University of Maryland, College Park, MD 20742, United States



ARTICLE INFO

Article history:

Received 2 May 2014

Received in revised form 21 January 2015

Accepted 24 January 2015

Available online 20 February 2015

Keywords:

Landsat

MODIS

Burned area mapping

Semantic change detection

Object-oriented data fusion

ABSTRACT

Fire products derived from coarse (500 m to 1 km) spatial resolution satellite data have become an important source of information for the fire science and applications communities. There is however a demand for moderate (30 m) spatial resolution burned area data sets, systematically generated at regional to global scale, that to date has been only partially met. This paper presents a methodology to fuse multi-temporal Landsat Enhanced Thematic Mapper plus (ETM+) data with Moderate Resolution Imaging Spectroradiometer (MODIS) active fire detections to map systematically burned areas at 30 m resolution. A multistage mapping approach is used with an initial per-pixel change detection based on spectral-rule based pre-classification of Landsat 30 m time series to identify candidate burned areas. The candidate burned area objects are then either retained or discarded by comparison with contemporaneous MODIS active fire detections. The methodology is demonstrated for 1.9 million km² over the Western United States using all the Landsat 7 ETM+ data and Terra MODIS active fire detections acquired in 2002. Systematic evaluation conducted by per-pixel and per-burned area object comparison with the burned area perimeters provided by the USGS Monitoring Trends in Burn Severity (MTBS) project is presented, and shows a good agreement in the identification of burning patterns but a likely underestimation of the total area burned. Future research to refine and further test the methodology is discussed.

© 2015 Elsevier Inc. All rights reserved.

1. Introduction

Coarse spatial resolution satellite data (500 m to 1 km) have been used extensively in the past decades to systematically monitor fire using computer algorithms to detect the location and intensity of active fires at the time of satellite overpass, and algorithms to map the spatial extent of the areas affected by fires (Mouillot et al., 2014; Roy, Boschetti, & Smith, 2013). Until the successful launch of the polar-orbiting coarse resolution Moderate Resolution Imaging Spectroradiometer (MODIS) sensors on the Terra and Aqua platforms there were no environmental satellite systems with dedicated fire monitoring capabilities (Justice, Smith, Gill, & Csiszar, 2003). The MODIS design includes bands selected for fire detection and well suited for burned area mapping, and MODIS data are used to systematically generate global coarse resolution daily 1 km active fire (Giglio, Descloitres, Justice, & Kaufman, 2003), monthly 500 m burned area (Giglio, Loboda, Roy, Quayle, & Justice, 2009; Roy, Jin, Lewis, & Justice, 2005), and associated global emission products (van der Werf et al., 2010). The MODIS product record will continue with the 2011 successful Suomi NPP Visible Infrared Imaging Radiometer Suite (VIIRS) launch and the planned follow-on Joint Polar Satellite Suite (JPSS)-1 VIIRS mission. VIIRS has dedicated active fire detection capabilities (Csiszar et al., 2014; Schroeder, Oliva, Giglio, & Csiszar, 2014) with a coarse spatial resolution of 750 m and 375 m for the thermal and

reflective wavelength bands respectively (Murphy, Ardanuy, Deluccia, Clement, & Schueler, 2006).

The need for moderate to high spatial resolution (10 m to 30 m) burned area products has been advocated by fire product users for applications including carbon budget accounting, estimation of pyrogenic emissions of greenhouse gasses, particulates and aerosols (GOFC-GOLD, 2014; Hyer & Reid, 2009; Mouillot et al., 2014; Randerson, Chen, van der Werf, Rogers, & Morton, 2012), fire management and post-fire remediation (Lentile et al., 2006; Rollins, 2009), and for environmental management applications (Justice et al., 2013; Trigg & Roy, 2007). Although moderate to high spatial resolution satellite data, such as provided by Landsat (Roy et al., 2014), ASTER (Yamaguchi, Kahle, Tsu, Kawakami, & Pniel, 1998) or RapidEye (Tyc, Tulip, Schulten, Krischke, & Oxford, 2005), provide the opportunity for detailed spatial mapping of burned areas, they have reduced temporal resolution due to their narrow field of view relative to coarse resolution polar-orbiting sensors such as MODIS or VIIRS. The temporal frequency of satellite acquisitions is very important for fire monitoring because the fire behavior and post-fire surface effects can change rapidly, and can be obscured by clouds, smoke and other optically thick aerosols (Giglio, 2007; Roy, Boschetti, Justice, & Ju, 2008; Smith & Wooster, 2005). In addition, disturbances such as shadows, flooding, crop harvesting, or rapid vegetation senescence may produce spectrally similar effects to burned areas in single

date images (Roy, Jin, et al., 2005). These issues present challenges to the automated classification of moderate to high spatial resolution satellite data.

Since 2008, the USGS has been distributing Landsat data at no charge via the Internet (Woodcock et al., 2008). This provides the opportunity for researchers to use all the data in the U.S. Landsat Data Archive and to consider Landsat data for long-term, large area, burned area monitoring. To date, Landsat data have not been used for this purpose, arguably because of the technical challenges discussed above and perhaps because of past Landsat data cost and processing limitations. A notable exception is the U.S. Monitoring Trends in Burn Severity (MTBS) project that is producing annual Landsat derived maps of burned areas for all the conterminous U.S. and Alaska (Eidenshink et al., 2007; Rollins, 2009). However, the mapping is performed by manual interpretation with a reporting lag of up to more than one year and only for burned areas greater than 2 km² and 4 km² in the Eastern and Western U.S. respectively (Eidenshink et al., 2007). In addition, unburned islands within the perimeters of burned areas are not always mapped (Sparks, Boschetti, Tinkham, Smith, & Lannom, 2015). Automated, computationally efficient algorithms are required for long time series, and continental to global coverage Landsat application, as Landsat algorithms that require high levels of user intervention are not scalable (Roy et al., 2014).

This paper presents a novel methodology to generate multi-temporal Landsat-based 30 m resolution burned area maps with the same degree of automation employed for systematic burned area mapping using multi-temporal coarse resolution MODIS data (Giglio et al., 2009; Roy, Jin, et al., 2005). The low 16-day Landsat revisit period prevents the reliable application of daily time series processing algorithms developed to generate coarse resolution global burned area products. In order to overcome the limitations posed by the inherent ambiguity of the spectral characteristics of burned areas, and by the limited temporal resolution of Landsat data, the methodology presented in this paper uses spectral changes in time series of Landsat 30 m data and temporally and spatially near-coincident daily 1 km MODIS active fire detections as separate sources of evidence for the occurrence of fire. A multistage mapping approach is used with an initial per-pixel change detection, performed on a spectral based rule pre-classification of the Landsat 30 m time series to identify candidate burned pixels, followed by their segmentation into candidate burned area objects, and then by an object-oriented fusion of the candidate burned area objects with MODIS 1 km active fire detections.

This paper first provides context for the developed burned area mapping algorithm, by overviewing relevant satellite burned area mapping and Landsat land surface change mapping approaches. This is followed by sections that describe the input data, the study area, and the burned area mapping methodology. Results are demonstrated for a year of MODIS and Landsat data for an extensive study area (~1.9 million km²) centered on the forested areas of the Western United States. The results are evaluated by comparison with MTBS manually mapped burned area perimeters. The paper concludes with a discussion of the potential steps for the refinement and expansion of the proposed methodology to continental and global scales.

2. Satellite burned area mapping overview

Satellite active fire detection algorithms provide information on the location of fires detected at the time of satellite overpass (Giglio et al., 2003). However, it is well established that the spatial extent of burning cannot be estimated reliably from active fire detections alone, as the satellite may not overpass at the time of day when burning occurs and because clouds and optically thick smoke may preclude active fire detection (Giglio, 2007; Roy et al., 2008; Smith & Wooster, 2005). Also, active fire detection probability is dependent on the fire temperature and size: small and cool fires may not be detected at the time of satellite overpass (Giglio et al., 2003; Schroeder et al., 2008). Typically,

cumulative active fire detection maps underestimate the area burned in grassland and savanna ecosystems where the fire front progresses rapidly across the landscape (Boschetti & Roy, 2009; Roy et al., 2008). Conversely, active fire detection algorithms may overestimate the area burned for isolated fire events that are detected but that are very hot and smaller than the pixel dimension, for example, in certain forest ecosystems where the fuel availability can sustain high energy release and the fire front progression is slow relative to the satellite overpass frequency (Giglio et al., 2006; Roy, Jin, et al., 2005).

The majority of burned area mapping algorithms attempt to detect spectral changes induced by fire: vegetation fires deposit charcoal and ash, remove or reduce the amount of photosynthetically active vegetation, alter the vegetation structure, and sometimes reveal the vegetation understory and soil (Barbosa, Gregoire, & Pereira, 1999; Pereira, Chuvieco, Beaudoin, & Desbois, 1997; Roy, Giglio, Kendall, & Justice, 1999; Trigg, Roy, & Flasse, 2005). These changes are amenable to optical wavelength remote sensing, although they vary in complex ways in space and time depending on the pre-fire vegetation structure and underlying soil reflectance, the combustion completeness of the fire, unburned leaf drop, vegetation regrowth and recovery after the fire, and the geometry of observation (Chuvieco, Martín, & Palacios, 2002; Disney et al., 2011; Jin & Roy, 2005; Kokaly, Rockwell, Haire, & King, 2007; Lentile et al., 2006; López García & Caselles, 1991; Pereira & Setzer, 1993; Pereira et al., 1997; Roy & Landmann, 2005; Van Wagendonk, Root, & Key, 2004). Persistence of the charcoal and ash varies as a function of climate, fire regime and fuel load, while the burn scar signal duration depends on site primary productivity and vegetation recovery, and these effects can affect the multi-temporal detection of burned areas (Lhermitte, Verbesselt, Verstraeten, Veraverbeke, & Coppin, 2011; Pereira et al., 1997; Roy, Jin, et al., 2005; Trigg & Flasse, 2000).

It is not usually possible, in the absence of ancillary information, to unambiguously separate in a single image the spectral signature of burned areas from those caused by unrelated phenomena and disturbances such as shadows, flooding, snow melt, agricultural harvesting or ploughing (Roy, Jin, et al., 2005; Roy et al., 2008). In addition, the magnitude of spectral changes due to fire is dependent on the pre-fire conditions, including the amount, type, distribution and moisture of the vegetation fuel, and also on the fire behavior that depends on these conditions and factors such as temperature, wind and topography (Linn & Cunningham, 2005; Linn, Winterkamp, Edminster, Colman, & Smith, 2007). For these reasons, burned area mapping is complex and often highly site and time specific.

There are a number of global burned area products generated using coarse spatial resolution data predominately derived by application of time series change detection approaches to reflectance and/or spectral indices (Chuvieco et al., 2012; Giglio et al., 2009; Mouillot et al., 2014; Roy & Boschetti, 2009; Roy, Jin, et al., 2005; Tansey et al., 2004; Tansey et al., 2008). In most of these approaches, the high temporal resolution of coarse resolution polar-orbiting satellite systems (typically one or two days) is used to exploit the temporal persistence of burned areas, which can be observed on the ground for a period of several weeks (grasslands and savannas) to years (forests). Consequently, these approaches are generally ill-suited for processing Landsat data that nominally have a 16 day temporal resolution but are not always acquired or archived systematically, especially outside of the United States, and because of cloud obscuration at the time of Landsat overpass (Kovalskyy & Roy, 2013).

A number of hybrid burned area detection algorithms have been developed that integrate satellite active fire detections with reflective wavelength data to exploit the increased likelihood of a burned area occurring close to an active fire detection. Typically, the satellite active fire and reflectance data have similar spatial and temporal resolution and are defined using data sensed by the same sensor (e.g., MODIS or AVHRR) and the active fire detection location and date information are used to develop training data to characterize statistically the burned

pixels in terms of reflectance or spectral indices (George, Rowland, Gerard, & Balzter, 2006; Giglio et al., 2009; Roy et al., 1999), or the active fire detections are used as “seeds” in a region-growing algorithm applied to the reflectance or spectral indices (Fraser, Li & Cihlar, 2000; Fraser, Li & Landry, 2000; Loboda, O’Neal, & Csizsar, 2007; Maggi & Stroppiana, 2002; Pu, Gong, Li, & Scarborough, 2004).

There are a number of land cover change detection algorithms, designed to process Landsat pixel-level time series over large areas (Hansen & Loveland, 2012). These algorithms have focused primarily on mapping forest land cover change and forest disturbance using approaches that identify significant changes by examination of the temporal trajectory of surface reflectance or vegetation indices (Cohen, Yang, & Kennedy, 2010; Hansen et al., 2013; Huang et al., 2010; Kennedy, Yang, & Cohen, 2010; Kennedy et al., 2012; Masek et al., 2013; Meigs, Kennedy, & Cohen, 2011). The temporal trajectory is interpreted by per-pixel application of rules, which can be predefined, as in the Vegetation Change Tracker (Huang et al., 2010; Masek et al., 2013) and in the LandTrendr algorithms (Cohen et al., 2010; Kennedy et al., 2010, 2012; Meigs et al., 2011), or statistically derived from training data (Hansen et al., 2013). These algorithms allow for a characterization of the disturbance by differentiating between different types of temporal trajectory of the remotely sensed data, but do not report burned areas as a distinct category.

Landsat data have been used for burned area mapping for almost four decades; Lentile et al. (2006) and Roy et al. (2013) provide reviews of the wide variety of methods that have been proposed over the years. Arguably because of the high cost of Landsat data, most early research used highly specific classification techniques to map burned areas in a limited number of Landsat scenes (Koutsias & Karteris, 2000; López García & Caselles, 1991; Pu & Gong, 2004). The development of burned area techniques was often not the main focus of the research but rather a step to generate input data for fire ecology studies (Chuvieco & Congalton, 1988; García-Haro et al., 2001; Hall, Brown, & Johnson, 1978; Hall, Ormsby, Johnson, & Brown, 1980; Henry & Yool, 2002; Patterson & Yool, 1998), or for the validation of coarse resolution burned area products (Barbosa et al., 1999; Boschetti et al., 2006; Roy, Frost, et al., 2005; Sa et al., 2003; Silva, Sá, & Pereira, 2005; Smith et al., 2007). More recently, Landsat burned area mapping techniques have been developed which have the potential for application across different ecosystems, but they involve using carefully selected cloud-free images with some degree of human intervention or parameter tuning (Bastarrika, Chuvieco, & Martin, 2011; Eidenshink et al., 2007; Henry, 2008; Mallinis & Koutsias, 2012; Stroppiana, Bordogna, Carrara, et al., 2012), or the collection of site-specific burned pixel training data (Bastarrika et al., 2011; Goodwin & Collett, 2014; Stroppiana, Bordogna, Boschetti, et al., 2012). Object-oriented mapping techniques have also been applied to burned area mapping, but using semi-

automated approaches, which require human intervention for tuning of one or more site-specific parameters (Gitas, Mitri, & Ventura, 2004; Wulder et al., 2009; Zhang et al., 2005).

3. Data

3.1. Web enabled Landsat data (WELD)

The Web Enabled Landsat Data (WELD) project generated temporally composited mosaics of the conterminous United States (CONUS) and Alaska using every Landsat 7 Enhanced Thematic Mapper Plus (ETM+) Level 1 Terrain Corrected (L1T) acquisition with cloud cover $\leq 80\%$ available from the U.S. Landsat archive (Roy et al., 2010). The WELD products are designed to provide consistent data that can be used to derive land cover and geo-physical and bio-physical products. The CONUS WELD Version 1.5 weekly products were used in this study for burned area mapping; CONUS seasonal and annual products were used to illustrate the results only. The products are defined in 5000×5000 30 m pixel tiles (2275 km^2) in the Albers equal area projection. They are generated from Landsat 7 ETM+ Level 1T data that has six reflective wavelength bands, blue ($0.45\text{--}0.52 \mu\text{m}$), green ($0.53\text{--}0.61 \mu\text{m}$), red ($0.63\text{--}0.69 \mu\text{m}$), near-infrared ($0.78\text{--}0.90 \mu\text{m}$), short-wave infrared ($1.55\text{--}1.75 \mu\text{m}$ and $2.09\text{--}2.35 \mu\text{m}$), and two thermal bands (both $10.40\text{--}12.50 \mu\text{m}$ with low and high gain settings). The Level 1T data processing includes radiometric correction, systematic geometric correction, precision correction using ground control chips, and the use of a digital elevation model to correct parallax error due to local topographic relief. The L1T ETM+ geolocation error in the CONUS is less than 30 m even in areas with substantial terrain relief (Lee, Storey, Choate, & Hayes, 2004). The WELD product data include, for each pixel, the Landsat top of atmosphere (TOA) reflectance, TOA brightness temperature, TOA normalized difference vegetation index (NDVI), the date each composited pixel was acquired on, the per-band radiometric saturation status, two cloud mask values, and the number of acquisitions considered in the compositing period (Roy et al., 2010).

The weekly, rather than monthly or seasonal, WELD products were used for burned area mapping to obtain the richest temporal Landsat 7 ETM+ time series. The Landsat 7 ETM+ has a 15° field of view that captures moderate spatial resolution scenes over a $\sim 183 \text{ km} \times 170 \text{ km}$ extent defined in a Worldwide Reference System (WRS) of path (groundtrack parallel) and row (latitude parallel) coordinates (Arvidson, Goward, Gasch, & Williams, 2006). Every daytime sunlit Landsat 7 ETM+ overpass of the CONUS is ingested into the U.S. Landsat archive, a total of 455 unique path/rows, with an annual maximum of 22 or 23 acquisitions per path/row and an annual mean cloud cover of about 40% (Ju & Roy, 2008). Each Landsat path is acquired every 16 days, and adjacent paths are acquired 7 days apart. Over the

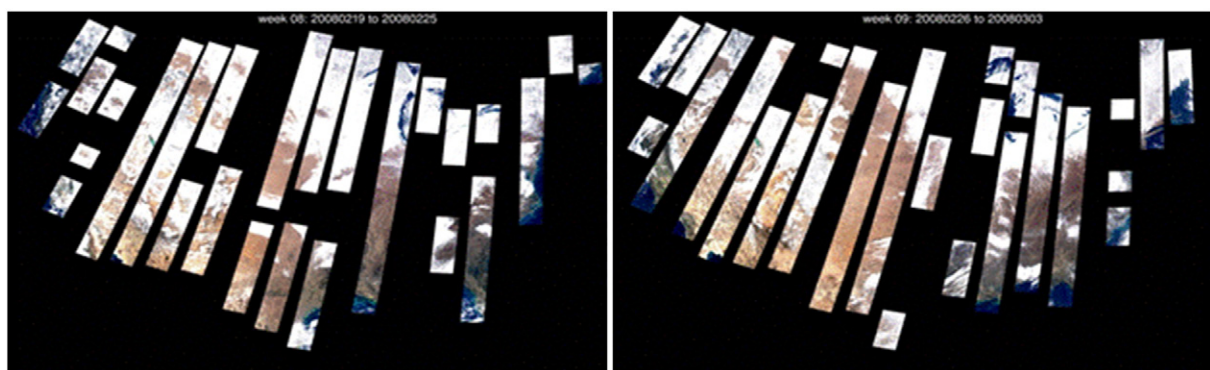


Fig. 1. Two consecutive weekly WELD products over the conterminous United States, true color top of atmosphere reflectance, 2006 weeks 8 (left) and week 9 (right). The black gaps within sensed Landsat paths (the NE to SW strips) occur where the L1T image cloud cover was greater than 80% and so were not WELD processed.

CONUS the weekly WELD products never contain more than one Landsat acquisition per 7 day period and so no information is lost due to temporal compositing. This is clearly apparent in Fig. 1.

3.2. MODIS active fire product

The MODIS active fire product detects fires in 1 km MODIS pixels that are actively burning at the time of satellite overpass under relatively cloud-free conditions (Giglio et al., 2003). The Collection 5, Level 3 8-day MODIS Terra active fire product (MOD14A1) was used in this

study. The MOD14A1 product is defined in the standard MODIS Level 3 Land tile format in the sinusoidal projection (Wolfe, Roy, & Vermote, 1998). It contains 8 daily active fire detection summaries stored as separate bands defining for each 1 km pixel if an active fire was detected within the 24 hour period. In the absence of fires, it reports if there were any MODIS observations in the same 24 hour period, if any of these were cloudy, or if not cloudy if the surface was land or water (Giglio et al., 2003). For each active fire detection a confidence level (high, medium, and low) is also stored. At CONUS latitudes the MODIS Terra overpasses once per day and once per night and so provides

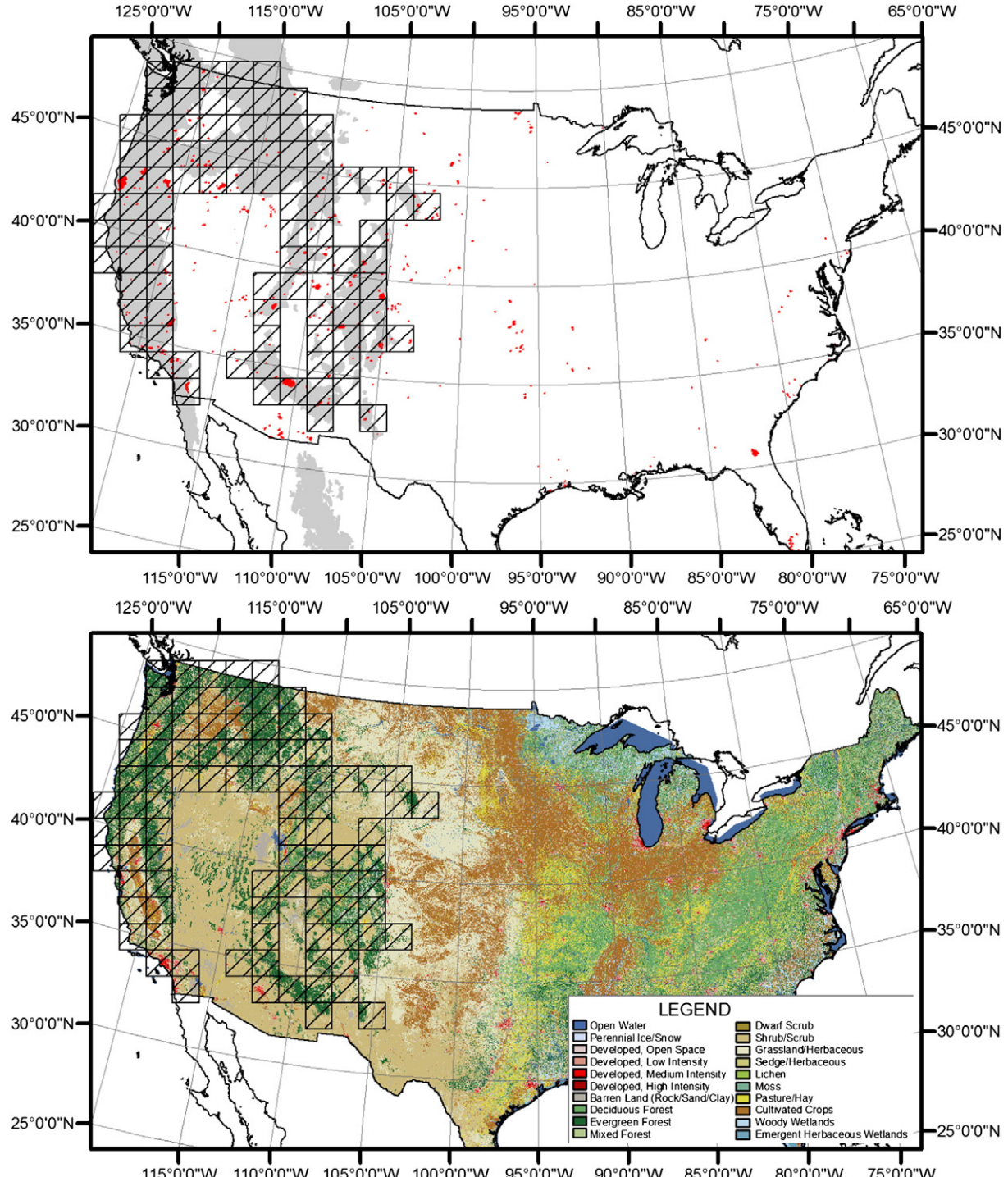


Fig. 2. Study area. Top: the 92 150 × 150 km WELD tiles (diagonal hatch), MTBS mapped burned areas for 2002 (red) and forested ecoregions (gray) over the Western United States (Northwestern Forest, Marine West Coast Forest, Mediterranean California, Temperate Sierras). Bottom: the 92 WELD tiles overlain on the NLCD 2001 landcover map of the United States.

much more frequent sensing compared to the nominal 16 day Landsat observation frequency.

3.3. Monitoring trends in burned severity (MTBS) burned area perimeters

The MTBS burned area perimeters were used in this study to validate the 30 m burned area products. The MTBS project, carried out by the USGS National Center for Earth Resources Observation and Science (EROS) and the USDA Forest Service Remote Sensing Application Center (RSAC), produces annual burned area and fire severity maps for the conterminous United States and Alaska from 1984 to the present date. Only burned areas larger than 1000 acres ($\sim 4 \text{ km}^2$) in the Western U.S. and larger than 500 acres ($\sim 2 \text{ km}^2$) in the Eastern U.S. are mapped. The burned area perimeters are mapped by on-screen expert interpretation of Landsat data and using U.S. forest service ancillary ground

information when available (Eidenshink et al., 2007). To streamline the visual interpretation the analysts are not required to map unburned islands within the outer polygon of each burned area, sometimes resulting in an overestimation of the area burned (Sparks et al., 2015). The MTBS project was designed with a primary focus on land management support, and not on the production of unbiased burned area estimates (Eidenshink et al., 2007). Despite these limitations, the MTBS product is a wall-to-wall, manually generated Landsat resolution burned area map of the United States, and comparing it to the results of the proposed methodology provides useful insight on its overall performance.

3.4. Data pre-processing

All the daily MODIS active fire detections, the MTBS data, and the corresponding 52 weekly WELD products for a single year were

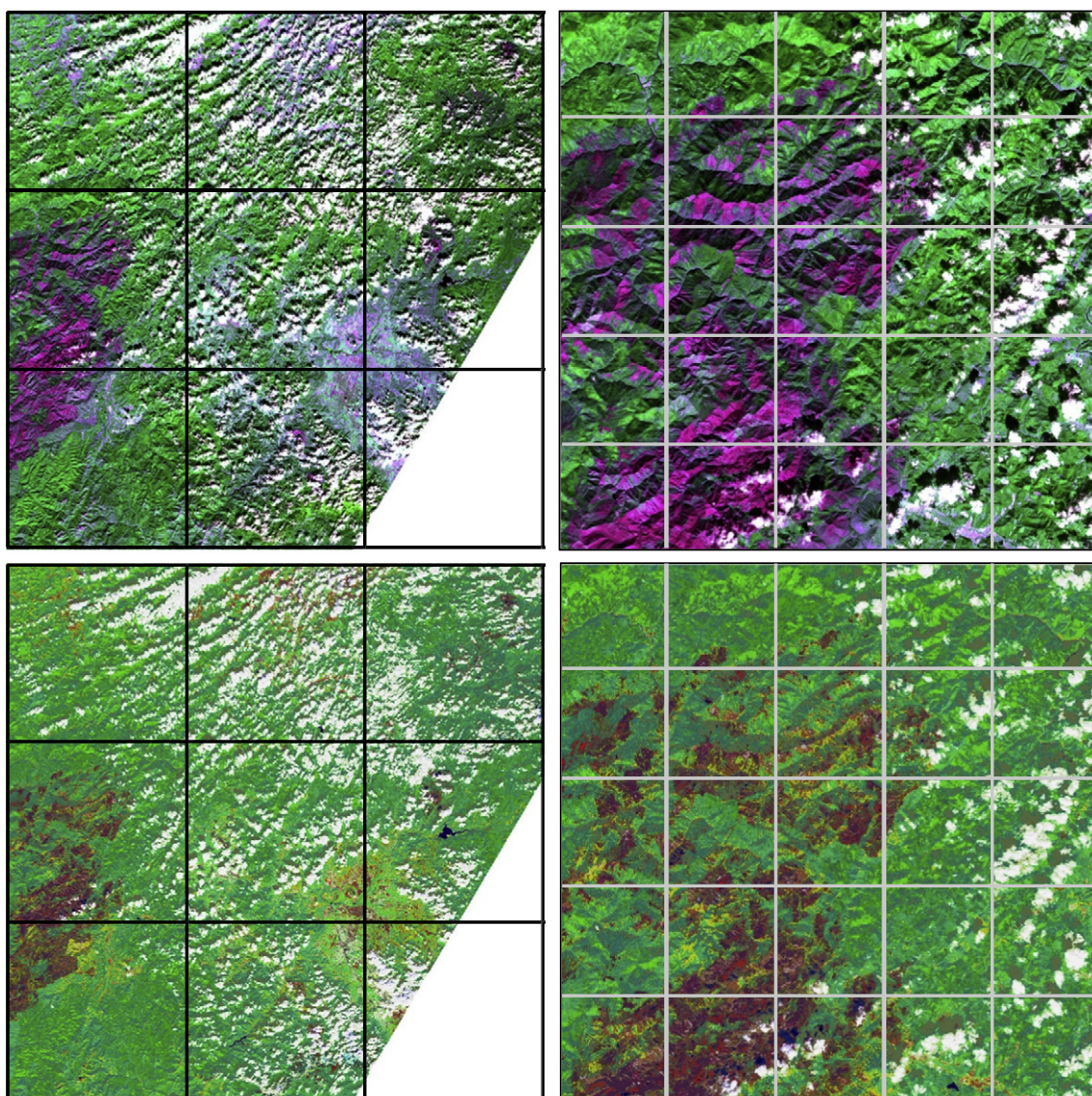


Fig. 3. Example weekly WELD product (top row) and corresponding spectral categories (bottom row) for a full $150 \times 150 \text{ km}$ WELD weekly tile (left column) and a $50 \text{ km} \times 50 \text{ km}$ spatial subset (right column). The geographic coordinates of the full tile (tile h02v05) are: $43.0129^\circ\text{N}, 124.3634^\circ\text{W}$ (upper left corner) and $42.1050^\circ\text{N}, 122.0814^\circ\text{W}$ (lower right corner); the geographic coordinates of the subset are: $42.6711^\circ\text{N}, 124.2192^\circ\text{W}$ (upper left corner) and $42.4321^\circ\text{N}, 123.6087^\circ\text{W}$ (lower right corner). To facilitate the comparison of features across figures, a 50 km grid is superimposed on the full tile (left column) and a 10 km grid is superimposed on the subset (right column). The weekly WELD data belong to week 40 of 2002 (Landsat data sensed on October 1st 2002) and encompass the eastern part of the 2002 Biscuit Fire in Southern Oregon. The WELD data are shown as a false color composite (red $2.09\text{--}2.35 \mu\text{m}$, green $0.77\text{--}0.90 \mu\text{m}$ and blue $1.55\text{--}1.75 \mu\text{m}$) that emphasizes the contrast between burned areas (magenta tones), soils (bright magenta and purple), and photosynthetically active vegetation (green tones). The 95 preliminary classification spectral categories are colored intuitively, with cloud categories displayed in shades of white and gray, high canopy cover vegetation in shades of green from bright green (high LAI) to dark green (low LAI), low canopy cover vegetation as yellow, bare soils as brown, and charcoal as purple.

used. The daily MOD14A1 data were reprojected from the MODIS sinusoidal projection into the WELD Albers equal area projection at 30 m resolution. The footprint of each MOD14A1 1 km active fire detection pixel was projected from sinusoidal coordinates into the Albers coordinate system and then all the WELD 30 m pixels falling within the projected footprint were labeled as fire for the day of MODIS detection. We note that the MODIS is a whiskbroom sensor with a 110° field of view with a complex point spread function, and the MODIS active fire product detects fires that occur in elliptical areas that increase in area from approximately 1 by 1 km at nadir to up to 2.0 by 4.8 km in the along-track and along-scan directions at scan edge respectively (Wolfe et al., 1998). However, for the purposes of the present study, the reprojection and resampling of the MOD14A1 pixel corners is sufficiently geometrically precise, as the MOD14A1 detections are used only to establish if there were active fires close in time and space to a Landsat potential burned area detection. The geolocation error between the Landsat and MODIS datasets can be considered negligible compared to the uncertainty in the position of the active fires within a MODIS pixel: the MODIS geolocation accuracy is within 50 m at nadir (Wolfe et al., 2002) and the Landsat geolocation accuracy is within 30 m in the United States (Lee et al., 2004). The MTBS data are available as vector polygons and so their reprojection onto the WELD geometry is straightforward. The MTBS polygons were converted to 30 m rasters in Albers Equal Area projection, and all the 30 m pixels falling within the MTBS polygons were labeled as burned.

4. Study area and temporal period of study

The study area covers the forested ecoregions of the Western United States defined using the Environmental Protection Agency (EPA) Level I ecoregions of North America that stratify the CONUS into 15 regions with similar ecological and climatic characteristics (Griffith & Omernik, 2009). All the WELD tiles that include at least 10% of any of the Western forested ecoregions were selected, a total of 92 150 × 150 km WELD tiles corresponding to approximately 20% of the land area of the Continental United States (Fig. 2). These data cover 1,892,074 km² of land and predominantly contain shrubland (36%), evergreen forest (30%), and grassland (15%), as defined by the 30 m resolution 2001 National Land Cover

Database (NLCD) (Homer, Huang, Yang, Wylie, & Coan, 2004). Fires in the study area are prevalent and are thought to be increasing in size, frequency and severity (Westerling, Hidalgo, Cayan, & Swetnam, 2006) and provide a significant contribution to the total atmospheric emissions in North America (Houghton, Hackler, & Lawrence, 1999; Lin et al., 2014; Liu, 2004; Wiedinmyer & Hurteau, 2010).

The study period was the calendar year 2002. The WELD project has currently made publicly available all the Landsat 7 ETM + processed over the CONUS and Alaska since 2003. In order to test the performance of the detection on Landsat data not affected by the gaps due to the Scan Line Corrector (SLC) failure, that occurred in 2003 and removed 22% of the Landsat pixels (Markham, Storey, Williams, & Irons, 2004), WELD Landsat 7 ETM + products for 2002 were generated for this study. MODIS Aqua products only became available in May 2002 (Masuoka et al., 2010) and so, to ensure consistency throughout the year, only the 2002 MODIS Terra 8-day active fire detection product was used.

5. Mapping methodology

The methodology uses temporal changes in Landsat 30 m spectral categories and temporally and spatially near-coincident 1 km MODIS active fire detections as separate sources of evidence of the occurrence of fire. First, a preliminary detection of potentially burned Landsat 30 m pixels is derived by examination of spectral category changes through time with lax criteria to minimize omission errors. Then potential burned 30 m pixels are segmented (grouped) into candidate burned area objects using temporal and spatial proximity criteria. Finally, by comparison with contemporaneous MODIS 1 km active fire detections, and iterative contextual analysis, the candidate burned area objects are either retained as confidently detected burned areas or are discarded. These steps are described below.

5.1. Preliminary detection of potentially burned Landsat 30 m pixels by examination of spectral category time series

5.1.1. Landsat preliminary classification into spectral categories

Spectral categories, which are preliminary classification labels with an information content higher than unlabeled, unsupervised data

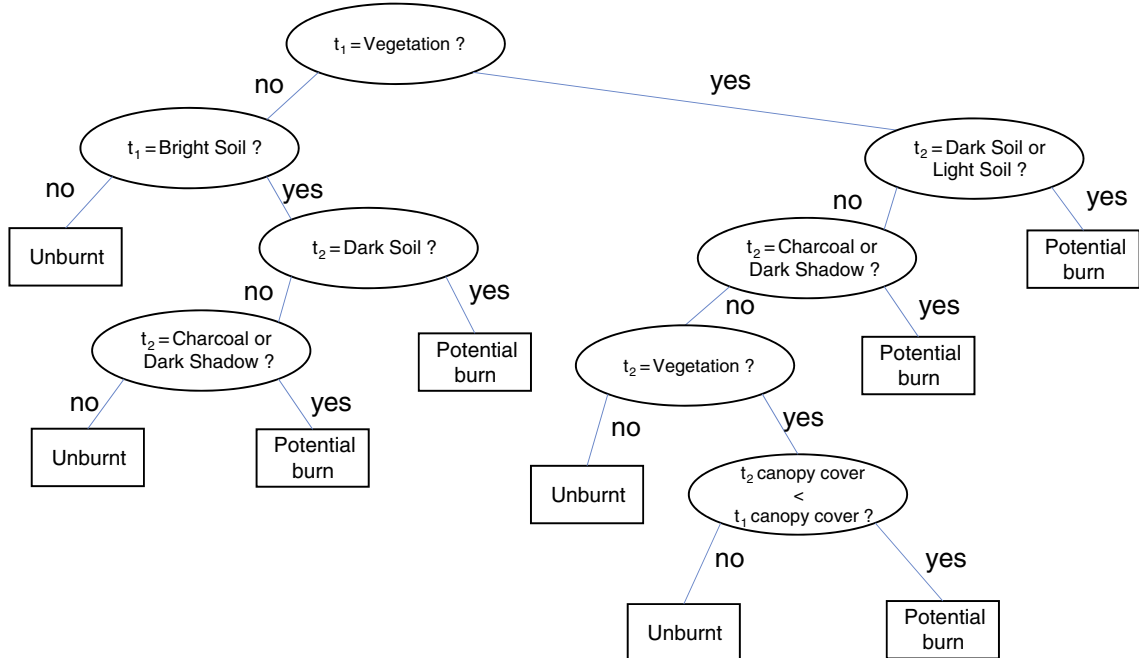


Fig. 4. Decision tree for the identification of potential burned Landsat 30 m pixels, implementing a semantic change detection strategy based on the analysis of the pixel-level spectral categories at two consecutive time steps t_1 and t_2 .

clusters, but equal to or lower than land cover class labels (Baraldi, Puzzolo, Blonda, Bruzzone, & Tarantino, 2006) are derived for each 30 m pixel of each WELD weekly tile product. This was achieved by application of the spectral rule preliminary classifier described by Baraldi et al. (2010, 2006). The spectral rule preliminary classifier is a decision tree classifier, based on prior knowledge of the spectral signature of surface types, which labels each pixel into a discrete set of spectral categories belonging to five main families of spectral signatures (vegetation, soils and mineral surfaces, water or shadows, snow and ice, clouds or smoke plumes) with an additional unclassified category. The spectral rule preliminary classifier requires as input multi-spectral data that have been radiometrically calibrated into TOA reflectance or atmospherically corrected surface reflectance and, if available, TOA brightness temperature or surface temperature. In the current implementation, it identifies for WELD Landsat ETM+ data a total of 95 spectral categories: 29 vegetation spectral categories covering different combinations of leaf area index (LAI) and canopy cover, 30 soil categories, 12 water categories, 7 cloud spectral categories, and 17 additional spectral categories representing miscellaneous surfaces not belonging

to the main groups, including certain artificial man-made surfaces, and notably for this study charcoal associated with recent burned areas. More details on the spectral categories are described in Baraldi et al. (2010, 2006).

Fig. 3 illustrates WELD TOA 30 m reflectance (top row) and corresponding spectral categories (bottom row) for a weekly WELD product tile located at the border between Oregon and California, in the Western United States. The data were generated from one Landsat ETM+ image acquired on October 1st 2002 shortly after the Biscuit Fire, which started in July 2002 and affected 2000 km² of forest over three months (Harma & Morrison, 2003). Portions of the Biscuit Fire burned area are evident along the western tile edge (Fig. 3 left column) and are also shown in detail (Fig. 3 right column). The burned areas were classified by the spectral rule preliminary classifier into spectral categories describing vegetation with low LAI (yellow), bare soil (brown), and charcoal (purple); the unburned areas were classified into high canopy cover vegetation (shades of green from bright green (high LAI) to dark green (low LAI)). Cloud and shadow categories are also apparent. The data are extensively cloud contaminated, which is representative

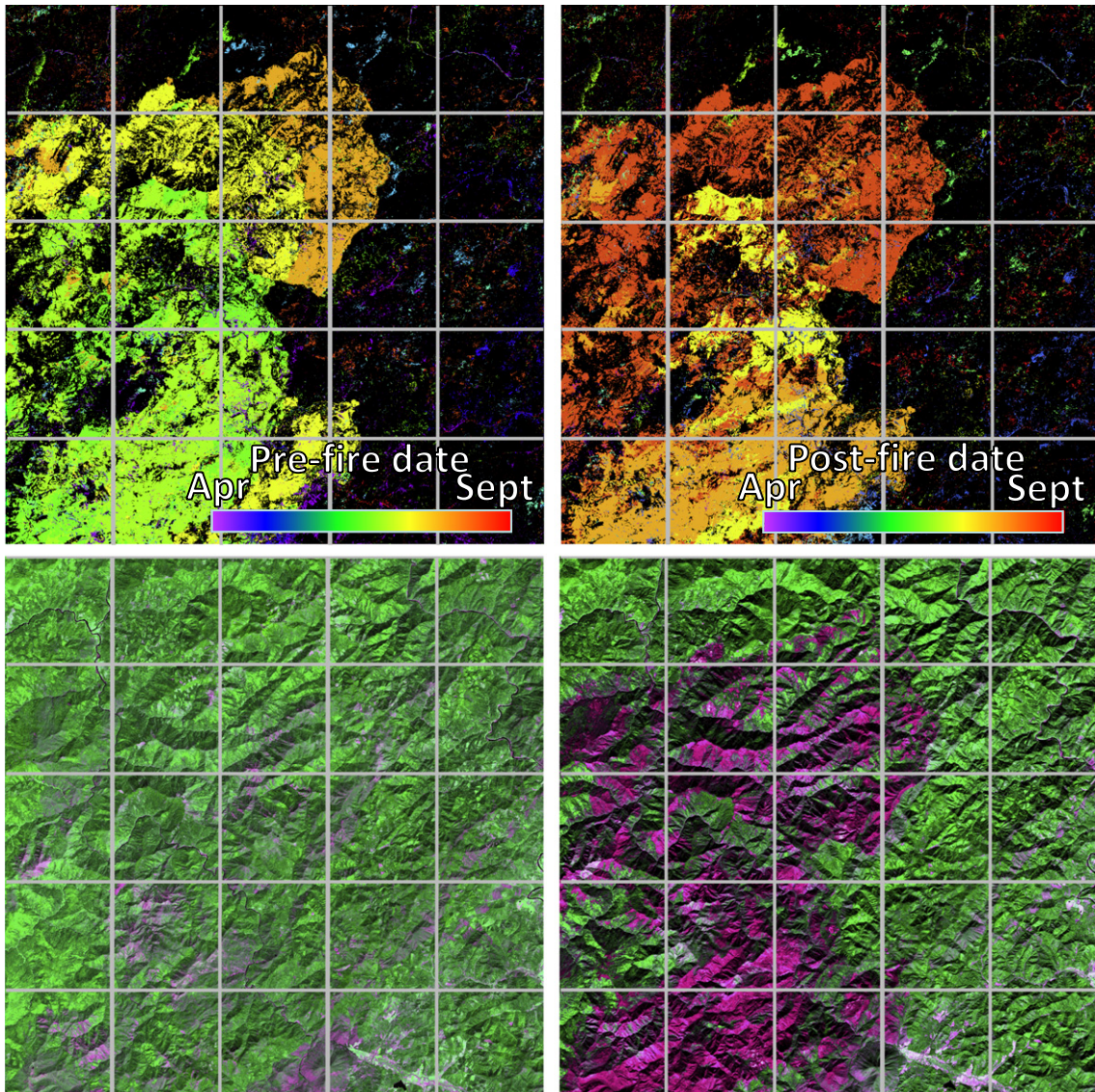


Fig. 5. 50 km × 50 km subset over the north-eastern part of the 2002 Biscuit Fire in Southern Oregon. Top row: Potential 2002 30 m Landsat burned pixels pre-fire (left) and post-fire (right) detection dates. Bottom row: Landsat false color composites (red 2.09–2.35 μm, green 0.77–0.90 μm and blue 1.55–1.75 μm) for the pre-fire (spring 2002, left) and post-fire (autumn 2002, right) seasonal WELD products that illustrate the change in reflectance due to burning and provide geographic context. The same 10 km grid of Fig. 3 is superimposed on the subset.

of cloud conditions for much of the U.S. at the time of Landsat overpass (Ju & Roy, 2008), and includes a region with no data acquired in the week due to the Landsat orbit geometry, illustrating the need for development of a Landsat burned area mapping methodology that is insensitive to these issues.

5.1.2. Detection of potentially burned Landsat 30 m pixels

A preliminary detection of potentially burned Landsat 30 m pixels is undertaken by examination of the spectral category time series at each WELD 30 m pixel location by the application of semantic rules concerning the temporal succession of spectral categories. This is different from the application of statistical thresholds or decision rules to spectral bands or derived spectral indices. For example, the removal of vegetation by fire followed by regrowth could result in a temporal sequence of spectral categories from “vegetation”, to “soil” or “charcoal”, to “vegetation”, while ephemeral flooding of a vegetated area could result in a temporal sequence from “vegetation”, to “water”, to “vegetation”. Notably, the temporal sequence of near-infrared (NIR) reflectance, or a vegetation index, for example the normalized difference vegetation index (NDVI), could provide very similar sequences for both cases, i.e., high NDVI to low NDVI to high NDVI, and potentially result in an ambiguous change interpretation.

The following semantic rules are applied to identify transitions between spectral categories that are compatible with burning. A potentially burned Landsat 30 m pixel is detected if two temporally consecutive spectral categories change as follows:

1. from any vegetation spectral category to any soil spectral category,
2. from any vegetation spectral category to a vegetation spectral category with lower canopy cover,
3. from any vegetation spectral category to a charcoal spectral category,
4. from a light soil spectral category to a dark soil or charcoal spectral category.

These semantic decision rules can be conceptualized as a decision tree, shown in Fig. 4, codified through a series of conditional tests on the spectral categories at consecutive time steps t_1 and t_2 . The tests are applied independently to each 30 m WELD pixel-level time series to generate a binary 30 m map of potentially burned and unburned pixels. The rules are purposefully broadly specified to minimize burned area omission errors at this initial stage, although they may also capture changes not associated with fire, such as, for example, cloud or relief shadows, crop harvesting or vegetation senescence. This however is not undesirable as MODIS 1 km active fire detections are used subsequently (Section 5.3) to eliminate commission errors and not to correct omission errors by adding new burned areas.

The semantic decision rules are applied to the 52 weekly WELD products independently for each gridded 30 m pixel location considering successive weeks through the time series until a potential burn is found or no potential burn is found over the year. In the presence of gaps in the time series due to clouds (as detected by the preliminary classification), or when there is no Landsat overpass, the first available observation after the gap is used. A pixel is assumed to not burn more than once per year, which is a reasonable assumption for the study area.

For each potential burned pixel, the Julian day of the pre-fire Landsat observation and the Julian day of the post-fire Landsat observation are stored. This information is needed for the subsequent MODIS active fire comparison. Fig. 5 shows a 35 × 35 km detail of the Southern Oregon burned area illustrated in Fig. 3, showing the pre-fire and the post-fire detection dates of the potential burned pixels derived by application of the semantic rules to the 52 weekly 2002 WELD products. For geographic context the seasonal Spring and Fall WELD 30 m three-month composites for this region are also shown as their data were sensed before and after the fire started. Visual comparison of the potential burned area detection pre- and post-fire detection dates (top row) with the pre-fire and post-fire seasonal images (bottom row) indicate commission errors outside the fire perimeter; this is a direct consequence of

the lax semantic rules adopted for the detection of the potentially burned pixels. In addition, some omission errors are also apparent and likely occur because pixels that had a small fraction burned and/or that burned with low combustion completeness will exhibit only a small post-burn change in reflectance (Roy & Landmann, 2005). Even with lax semantic rules, these pixels will likely not be selected as potential burned area detections.

5.2. Segmentation of potentially burned Landsat 30 m pixels into candidate burned area objects

The individual potentially burned 30 m pixels are segmented (grouped) into candidate burned area image-objects using temporal and spatial proximity criteria. An image-object (henceforth termed for convenience an ‘object’) is generally defined as a discrete region of an image, consisting of a set of pixels that is internally coherent and different from its surroundings according to predefined criteria (Hay & Castilla, 2008). The potentially burned Landsat 30 m pixels are segmented into candidate burned area objects based on their spatial adjacency and the coherence of the temporal detection interval using a spatio-temporal segmentation approach similar to the one described in Boschetti and Roy (2009).

The spatial adjacency is established by requiring that each 30 m potentially burned pixel in an object shares an edge or a corner with at least one other potential burned pixel in the object (i.e., using an 8-pixel neighborhood); the original implementation of the two pass connected component segmentation algorithm (Sonka, Hlavac, & Boyle, 2008) used for this processing step is described in Baraldi and Boschetti (2012). The temporal adjacency is established by requiring that all potentially burned pixels in an object have the same pre-fire and the same post-fire observation dates. In this way it is possible to associate a single detection interval to each object, enabling the subsequent object-oriented fusion with the MODIS active fire detections. Fig. 6 shows the result of applying the spatio-temporal segmentation to the pre-fire and the post-fire detection dates of the potentially burned pixels illustrated in Fig. 5. It is evident that because fires take time to progress across the landscape, and may be partially obscured

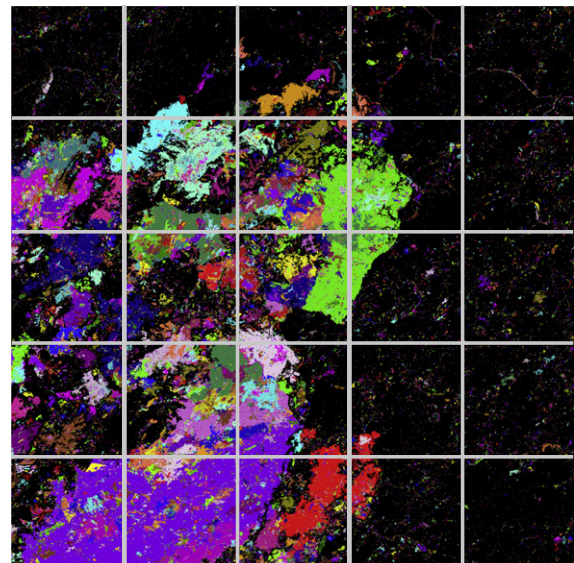


Fig. 6. Segmentation into candidate burned area objects of the potential burned area detections of the 50 km × 50 km subset over the north-eastern part of the 2002 Biscuit Fire (Fig. 5 top row). The colors, assigned randomly, denote different candidate burned area object labels. The same 10 km grid of Fig. 3 is superimposed on the subset.

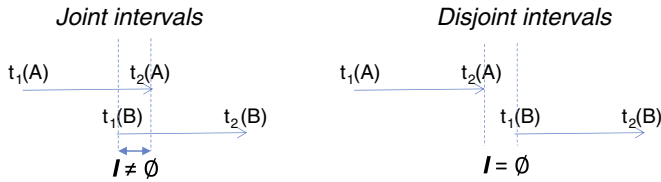


Fig. 7. Graphic example of the temporal adjacency test. Given an object A which is already a confidently detected burned area, a spatially adjacent object B is also considered confident if the two temporal detection intervals overlap. *Left:* the two intervals overlap ($I \neq \emptyset$), and object B is also considered a confident burned area. *Right:* the two intervals do not overlap ($I = \emptyset$) and object B is not considered a confident burned area.

by clouds, spatially adjacent pixels can have different pre-fire or post-fire Landsat 30 m detection dates, and so may be assigned to different adjacent candidate burned area objects.

5.3. Candidate burned area object rejection or confirmation by examination of contemporaneous 1 km MODIS active fire detections

An iterative process that examines the spatio-temporal proximity of the candidate burned area objects to contemporaneous MODIS 1 km active fire detections is undertaken, resulting in each candidate object being either retained as a confident burned area or discarded as a commission error.

First, each candidate burned area object is considered as confidently identified if it spatially overlaps, entirely or partially, with the footprint of at least one MODIS active fire detection and if its pre-fire and post-fire dates encompass the MODIS active fire detection date. In this process, all the active detections are used regardless of the detection confidence (low, medium, high) to provide the greatest number of active fire detections. It is reasonable to assume that when a low confidence active fire is coincident in time and space with a Landsat spectral change potentially due to fire, then the convergence of evidence indicates a real fire event. However, it is not reasonable to assume that at least one MODIS active fire observation will always be available to identify a genuine burned area object because of the limited MODIS diurnal sampling (two

MODIS Terra observations per 24 h at the study area latitudes) and because of the potential presence of obscuring clouds at the time of active burning.

To avoid discarding genuine burned areas, the following contextual analysis of the remaining candidate burned area objects is conducted. Candidate objects are considered as confidently burned if they are adjacent in both space and time to one or more objects which were confidently identified in the previous step. This assumes that if candidate burned area objects are spatially adjacent with similar pre-fire and post-fire dates, then the fire could have moved from one object to the other. The spatial adjacency is defined using an 8-pixel neighborhood, requiring that two objects share a pixel edge or a corner. The temporal adjacency is defined by requiring that the detection intervals of the two objects overlap. The intersection I of the two temporal intervals is defined as:

$$I = [t_1(A), t_2(A)] \cap [t_1(B), t_2(B)] \quad (1)$$

where $[t_1(A), t_2(A)]$ and $[t_1(B), t_2(B)]$ are the pre-fire and post-fire detection dates of candidate burned area objects A and B respectively. If I is a positive time interval ($I \neq \emptyset$), there is temporal adjacency, if I is a null set ($I = \emptyset$) there is no temporal adjacency. This test is illustrated in Fig. 7 for examples that satisfy and do not satisfy the temporal adjacency requirement.

The contextual analysis is iterated until convergence is reached and no new candidate objects are labeled as confident burned areas between the successive iterations. Those objects that by the end of the iterative process have not been labeled as confident are discarded as commission errors.

Fig. 8 shows all the 2002 MOD14 active fire detections and the final 30 m mapped burned area for the Biscuit Fire subset. Comparing Figs. 8 and 5 it is evident that the 1 km MODIS active fire detection resolution is inadequate to define reliably the extent of the area burned, with systematic overestimation due to the large MODIS pixel footprint dimensions, and also some underestimation likely due to no fires actively burning or being observable at the time of MODIS overpass. The 30 m burned areas, resulting from the initial fusion with the MODIS active fire detections and the subsequent contextual analysis, are displayed

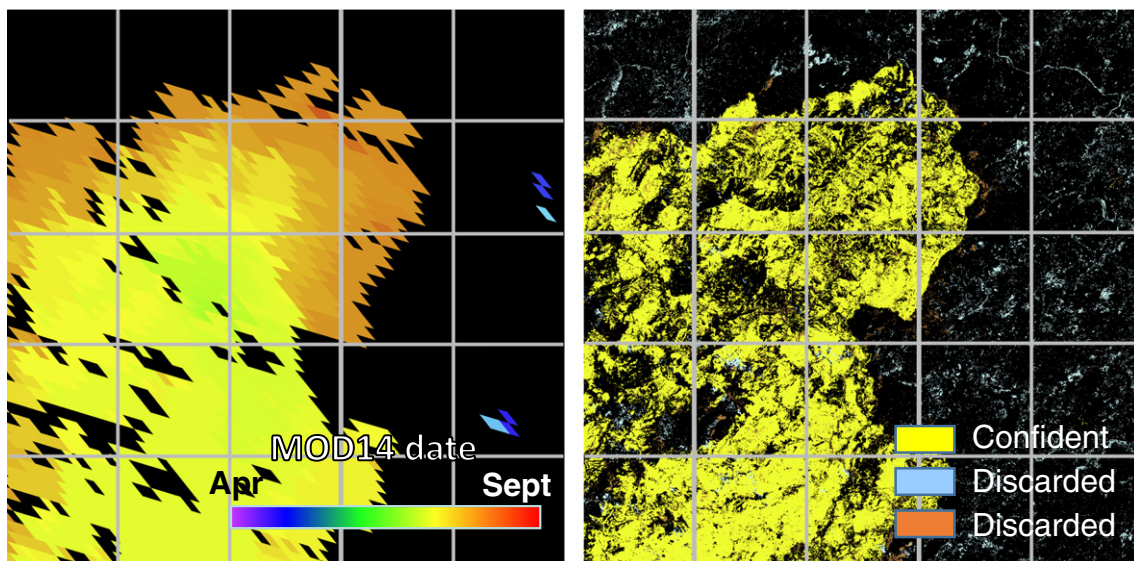


Fig. 8. Left: MODIS active fire detections resampled to 30 m and colored using the same rainbow color scale as the 30 m potential burned area detections for the 50 × 50 km subset over the north-eastern part of the 2002 Biscuit Fire illustrated in Fig. 5 (top row). Right: Results of the contextual analysis conducted on the candidate burned area objects shown in Fig. 6. Yellow: confident burned area objects; Orange: objects discarded because they overlap spatially, but not temporally, with active fire detections; Cyan: objects discarded because they are not temporally and spatially adjacent to confidently detected objects. The same 10 km grid of Fig. 3 is superimposed on the subset.

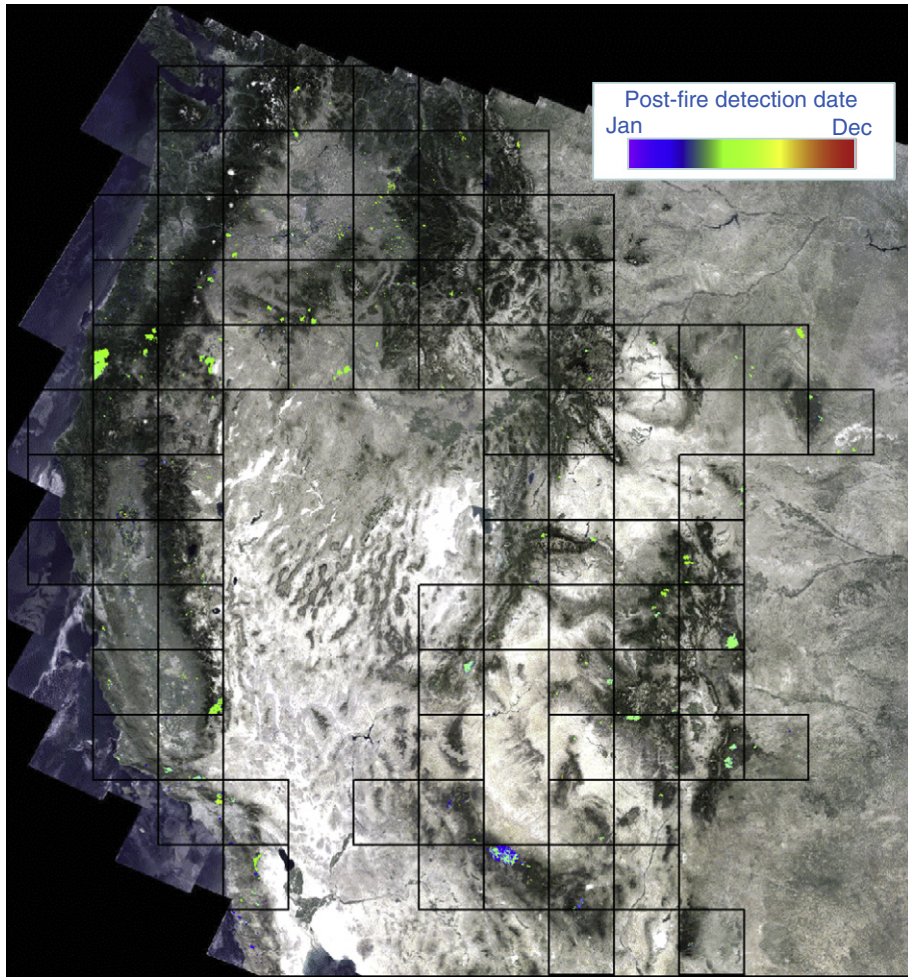


Fig. 9. Mosaic of the confidently detected 30 m burned areas, displayed with a rainbow color scale illustrating the first Landsat post-fire detection date. The outlines of the study area WELD tiles (Fig. 2) are shown in white. The true color 2002 WELD annual composite is shown as a background to provide geographic context.

in yellow, and exhibit spatial and temporal coherence with the pre-fire and post-fire Landsat images (Fig. 5 bottom row); both the outer perimeter of the burned area and the many interior unburned islands appear correctly identified. The candidate burned area objects discarded after the contextual analysis are displayed in green and red. The green colored objects show candidates that were neither temporally nor spatially adjacent to a confidently detected burned object and typically occur further away from confidently mapped burned areas. The red colored objects show candidates that, although overlapping spatially with the MODIS active fire detections, did not pass the temporal adjacency test [1].

6. Study area results

The methodology was applied independently to each 30 m pixel in each of the 92 study area WELD tiles (Fig. 2). Fig. 9 shows all the confidently detected burned areas, displayed with a rainbow color scale illustrating the first Landsat post-fire detection date, and overlaid on a true color WELD mosaic to provide geographic context. A total of 6811 km² was detected as burned in the study area for 2002, corresponding to 0.4% of the 1,892,074 km² land area. More than 65% of the area burned was detected between the beginning of July and the end of October (Fig. 9, green shades). Comparison with the NLCD 2001 landcover

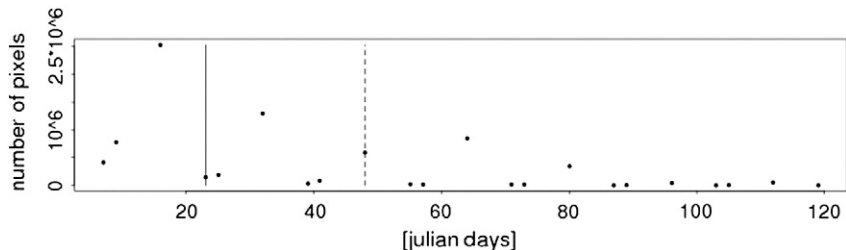


Fig. 10. Histogram of the temporal interval between the pre-fire and post-fire Landsat observation dates for the 30 m mapped burned areas (Fig. 9). The solid and dotted vertical lines show the median (23 days) and 75th percentile (48 days) time interval.

Table 1

Confusion matrix between the 30 m mapped burned areas (Fig. 9) and the rasterized 30 m MTBS polygons. For convenience, the matrix reports each entry as areal extent in km² rather than pixel counts (one 30 m Landsat pixel corresponds to 0.009 km²).

30m mapped burned areas				Omission error
MTBS reference data	Burnt [km ²]	Unburnt [km ²]	ROW TOTAL [km ²]	
Burnt [km ²]	5820.1	6126.4	11946.5	0.513
Unburnt [km ²]	938.2	1879189.7	1880127.9	0.000
COLUMN TOTAL [km ²]	6758.3	1885316.1	Total: 1892074.4 km ²	
Commission error	0.139	0.003	Overall accuracy: 0.999	

product indicates that the majority of the mapped burned areas occurred in evergreen forest (4145 km², corresponding to 61% of the total detected burned area), followed by shrublands (1485 km², 22% of the total), and grasslands (472 km², 7% of the total). Most of the detected 30 m burned pixels (87%) were found by direct comparison with the MODIS active fire detections; the remaining 13% were found by the contextual object-oriented analysis. This is primarily because the majority forest land cover that burned had fires that lasted for several days and so were detected by the MODIS active fire product.

The Landsat temporal resolution limits the precision of the estimate of the day of burning. In the ideal case of no missing observations the uncertainty is equal to the interval between two consecutive Landsat overpasses, i.e., 16 days at the center of a Landsat swath, and 7 or 8 days at the swath edge where neighboring Landsat swaths may overlap. Fig. 10 shows a histogram of the difference between the pre-fire and the post-fire detection date for all the detected burned area pixels (Fig. 9). The time differences are integer combinations of the revisit time of Landsat observations i.e., 7, 8 and 16 days, with a median difference of 23 days. The 75% percentile and maximum difference were 48 and 112 days respectively. This implies that, burned areas where the spectral response recovers rapidly, for example due to dissipation of charcoal and ash by the elements or vegetation regrowth, will not be detected under persistently cloudy conditions.

A systematic evaluation of the results was conducted by comparing them with the 2002 MTBS burned area perimeters. The MTBS dataset

has limitations, most notably the absence of interior unburned islands, which prevent its proper use as a validation dataset following the requirements of the standard protocol on burned area validation defined by the Committee on Earth Observing-Satellite Land Product Validation Subgroup (Boschetti, Roy, & Justice, 2009). However, it is the only wall-to-wall, Landsat scale burned area product available for the entire study area, and because it is produced by visual interpretation with rigorous quality control (Eidenshink et al., 2007; Rollins, 2009), it enables meaningful evaluation of the results of the current methodology. Table 1 shows a two-way confusion matrix computed by pixel comparison of the 30 m burned area map with the 30 m MTBS burned area data for the 92 WELD tiles. The total MTBS burned area (11,946 km²) was almost twice the Landsat burned area (6758 km²). Consequently the omission error was high (0.51) while the commission error was quite low (0.14) for the burnt class. Fire affects only a small fraction of the landscape in the continental United States (less than 1% according to both datasets), therefore the high overall classification accuracy can be explained by the predominance of the unburnt class.

Fig. 11 shows in detail the mapped burned area and MTBS burned area perimeter (left) and the post-fire WELD autumn composite (right) over the Biscuit Fire. The presence of unburned vegetation within the MTBS perimeter is clearly evident, and might partially explain why the total study area MTBS mapped burned area was greater than the Landsat mapped burned area. Indeed, shrub-steppe MTBS burned area perimeters have been found to systematically overestimate the area burned, with commission errors ranging from 4% to 18% compared to a reference dataset that correctly mapped unburned areas (Sparks et al., 2015).

The confusion matrix results (Table 1) summarize the pixel-level comparison between the products, but do not provide information on the spatial distribution of the areas of agreement and disagreement. In particular, it is relevant to understand whether the discrepancy in the total area burnt is mostly due to the presence of unburned vegetation within the MTBS polygons, or to the missed Landsat-based detection of entire fire events. To this end, a second level of comparison was conducted for individual MTBS perimeters rather than individual 30 m pixels. Fig. 12 highlights the spatial relationship between the MTBS polygons and the Landsat results, showing which MTBS polygons

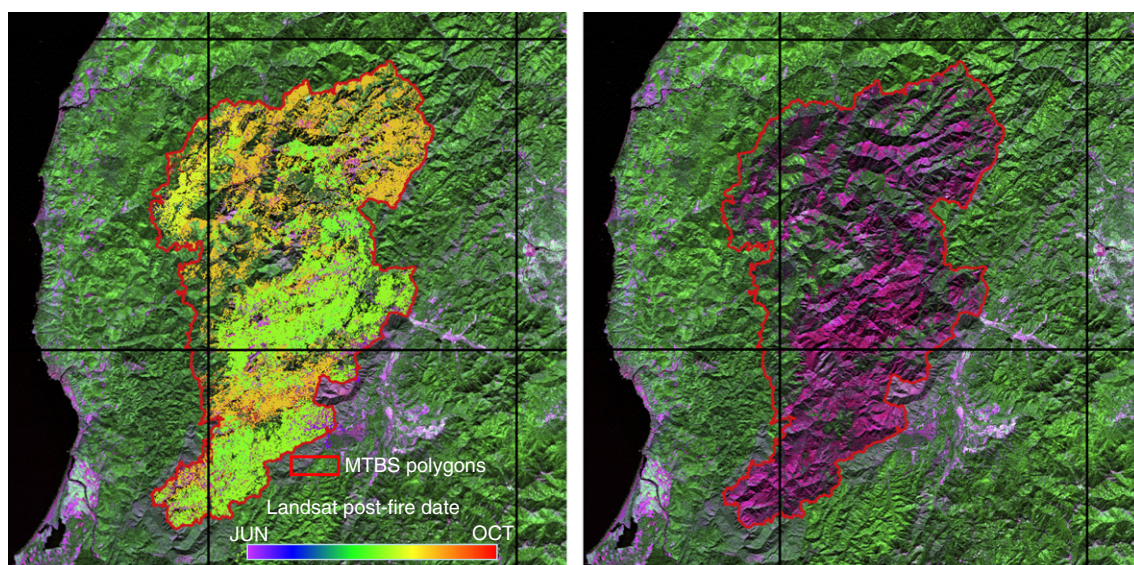


Fig. 11. A 90 km × 90 km region encompassing the Biscuit Fire in Southern Oregon. Left: Landsat burned area detections from the present study, displayed with a rainbow scale showing the first Landsat post-fire detection date, with MTBS perimeters (red vectors), overlaid on pre-fire (spring 2002) seasonal WELD product. Right: post-fire (autumn 2002) seasonal WELD product displayed in false color composition (red 2.09–2.35 μm, green 0.77–0.90 μm and blue 1.55–1.75 μm) to maximize the contrast between areas affected by the fire (magenta) and unburned vegetation (green). To facilitate the comparison of features across figures, the same 50 km grid of Fig. 3 is superimposed.

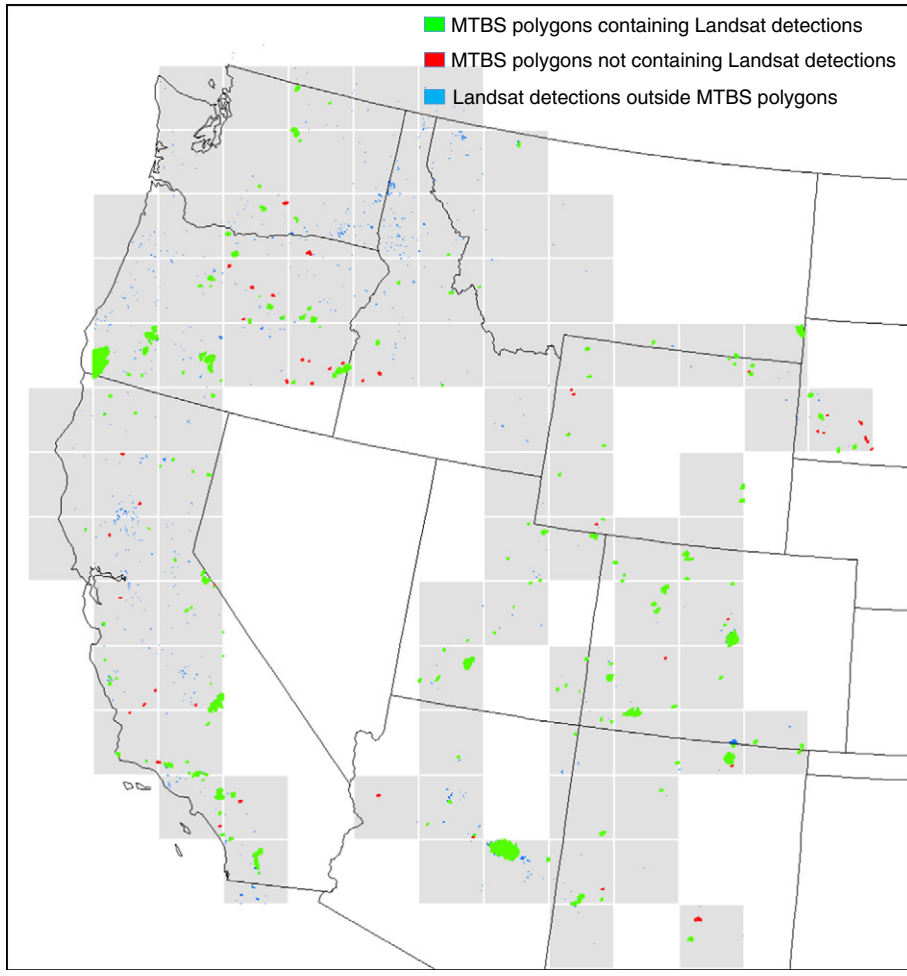


Fig. 12. Qualitative comparison between the MTBS burned area polygons and the 30 m Landsat burned area detections of the present study. The MTBS polygons that contain at least one Landsat detection are represented in green, the MTBS polygons that don't contain any Landsat detections are represented in red, and the Landsat detections that fall outside the MTBS polygons are represented in blue. The study area is shown in light gray, and the boundaries of the US states are plotted in black to provide geographic context.

overlap with the 30 m Landsat detections, and which polygons do not overlap. Of the 250 burned area polygons mapped by the MTBS project, 185 contained Landsat detections, and 65 did not.

The areas detected in the Landsat dataset but falling outside the MTBS polygons (blue in Fig. 12, i.e. potential commission errors) correspond to 13% of the total and are mostly small, under the 4 km² minimum mapping unit of the MTBS project. The 185 polygons that include Landsat detections (depicted in green) identify the greater majority of the area burned (97%), while the polygons that are entirely missed (depicted in red) cover only the remaining 3%. To further investigate

this, Table 2 summarizes the Landsat detection percentage with respect to six size intervals of MTBS polygons. The detection percentage increases with the size of the polygons, increasing from 55.4% for small burned areas (polygons under 10 km²) to 97.4% for larger ones (polygons between 30 km² and 100 km²) and then 100% for the largest ones (over 100 km²). The omission of entire polygons is largely a direct consequence of the use of MODIS active fire information to confirm candidate burned area detections: 61 of the 65 MTBS polygons missed by the Landsat classification did not contain any overlapping active fire detection.

Table 2

Frequency distribution of the MTBS polygon burned areas in the study area (Fig. 12). Six size intervals (from small burned areas to large burned areas) are defined on a logarithmic scale; for each size interval, the total number of MTBS polygons, and the number that overlapped spatially with one or more 30m Landsat detections (considered as detected), and the detection percentage are tabulated.

MTBS polygon burned area (a) [km ²]	Total number of MTBS polygons in the study area (n)	Number of MTBS polygons detected as burned using the Landsat–MODIS methodology ($n_{detected}$)	Percent detected $\frac{n}{n_{detected}} \times 100$
$a < 10$	128	71	55.4%
$10 \leq a < 30$	62	55	88.7%
$30 \leq a < 100$	39	38	97.4%
$100 \leq a < 300$	15	15	100%
$300 \leq a < 1000$	4	2	100%
$1000 \leq a < 3000$	2	2	100%

7. Discussion and conclusions

This paper presented a methodology to fuse Landsat 30 m spectral reflectance time series with contemporaneous MODIS 1 km active fire detections to generate large area 30 m burned area maps. The methodology attempts to overcome the limitations of the 16 day Landsat temporal resolution by incorporating daily MODIS active fire detections. It was demonstrated by processing a large annual dataset centered on the forested ecoregions of the Western United States that covered predominantly shrubland (36%), evergreen forest (30%), and grassland (15%). Comparison with independently derived MTBS burned area perimeters showed the absence of systematic commission errors due to spectral changes unrelated to fire, and a good agreement in the identification of regional burning patterns (Fig. 12). Further research to validate the product will be required, ideally using independent burned area reference data which complies with the CEOS Cal Val burned area validation protocol (Boschetti et al., 2009). The comparison with MTBS perimeters quantified a significant discrepancy in areal estimates between the two datasets; while this discrepancy can be partially attributed to the inclusion of unburned islands within the MTBS burned area perimeters (Sparks et al., 2015), omission errors may also be due to other factors, which are discussed below.

The precision in the temporal detection of the day of burning is limited by the 16 day temporal resolution of the Landsat data. Over the Western United States the observed uncertainty (median 23 days, 75th percentile 48 days) was significantly higher than the uncertainty of current coarse resolution products, for example, estimated for the MCD45 MODIS global burned area product as 1 day (median) and 4 days (75th percentile) (Boschetti, Roy, Justice, & Giglio, 2010). This is of particular concern, because areas where the vegetation recovery is more rapid than the interval between consecutive cloud-free observations may be missed by the present method. Use of contemporaneous Landsat 5 and Landsat 7 data, or of contemporaneous Landsat 7 and Landsat 8 data, would provide an 8-day repeat coverage and so enhanced probability of cloud-free surface observation (Kovalskyy & Roy, 2013; Roy et al., 2014). This combination would also reduce the reporting uncertainty and, by providing a denser time series, enable Landsat remote sensing closer to the fire event and therefore provide a stronger spectral category change, likely resulting in improved burned area detection.

A further limitation of the presented methodology is the requirement that at least one MODIS active fire detection partially overlaps with one or more temporally and spatially adjacent burned area candidate objects; analysis of the results showed that the omission of entire MTBS polygons can be largely attributed to the absence of coincident active fire detections. This has the potential of affecting not only the presented methodology, but all hybrid algorithms which use active fire detections combined with reflectance changes. While the test over the Western United States showed that the majority of fire events could be detected, previous global coverage research illustrates that in low tree cover ecosystems MODIS fire products significantly undersample the burning activity (Roy et al., 2008) and that small burned area patches are less likely than large patches to have any coincident active fire detections (Hanson, Padilla, Corti, & Chuvieco, 2013). New research will be undertaken to minimize this issue. First, incorporation of MODIS Aqua active fire detections will be investigated as the Aqua and Terra overpass times are different and so the two MODIS sensors combined provide more active fire detections per day. Incorporation of active fire detections from geostationary satellites that only detect very large and hot fires but every 15 to 30 min (Roberts & Wooster 1992; Zhang, Kondragunta, & Roy, 2014) will also be investigated. In addition, research to refine the semantic rule-based change detection will be conducted, for instance by further characterizing the preliminary candidate burned area detections according to the magnitude of spectral changes of suitable spectral band indices

(Bastarrika et al., 2011; Stroppiana, Bordogna, Boschetti et al., 2012; Stroppiana, Bordogna, Carrara, et al., 2012).

The WELD version 1.5 dataset, used for the input Landsat data, does not include any radiometric correction for the effects of topographic variations. This limitation may be among the causes of the omission errors observed in the results of the present study. The importance of topographic correction on land cover and burned area classification accuracy has been studied in previous work (Hanson & Chuvieco, 2011; Vanonckelen, Lhermitte, & Van Rompaey, 2013). However, systematic topographic correction, requiring both high resolution digital elevation models, and spatially and temporally accurate characterization of the atmosphere (Tanre, Herman, & Deschamps, 1981; Vermote & Kotchenova, 2008), is difficult to implement reliably over large areas and long time periods. None of the remote sensing top of atmosphere or surface reflectance Landsat datasets currently offer topographic correction (Masek et al., 2006; Roy et al., 2014). Further work to consider the persistence of post-fire changes with the assumption that shadows will not be persistent, following, for example, MODIS burned area time series algorithm approaches (Giglio et al., 2009; Roy, Jin, et al., 2005), will be investigated.

The research presented in this paper provides an approach to the generation of large area Landsat 30 m burned area maps, pathfinding the generation of multi-annual continental 30 m burned area products. The development was facilitated by the availability of geometrically corrected, preprocessed, and temporally composited Landsat data. The weekly WELD products preserve the information content of the original Landsat data, and eliminate the need to implement a dedicated pre-processing chain. Similar to the hierarchical approach followed in the development of the MODIS suite of land products (Justice et al., 2002), this research exemplifies how consistently processed and gridded data products are needed to enable the development of higher level Landsat thematic products (Roy et al., 2014). Importantly, no human interaction, i.e., no classification training data collection or visual interpretation, is required. Thus potentially the 30 m Landsat burned area mapping methodology can be applied on a systematic repeat basis with the same degree of automation as the MODIS global coarse resolution burned area product generation. The challenges to scaling the approach to global scale are predominantly in the refinement of the detection strategy to global environmental conditions and fire behaviors and also in dealing with the considerable data processing volume.

The proposed approach could also be developed to ingest contemporaneous remotely sensed data from additional sources: moderate resolution spectral reflectances from other sensors of the Landsat series (30 m Landsat 4 and 5 Thematic Mapper (TM) and Landsat 8 Operational Landsat Imager (OLI) data) or from the forthcoming Sentinel-2 mission (10 m and 20 m Multi-Spectral Instrument (MSI) data (Drusch et al., 2012)), and active fire detections from Aqua-MODIS, Suomi NPP VIIRS (Csizsar et al., 2014), Meteosat Spinning Enhanced Visible and Infra-Red Imager (SEVIRI) (Roberts & Wooster, 2008) and the forthcoming GOES-R Advanced Baseline Imager (ABI) (Schmidt, Hoffman, Prins, & Lindstrom, 2010). Fundamentally, using inputs from multiple remote sensing systems should provide more coherent and higher quality moderate resolution burned area maps, provided that there is consistent pre-processing and calibration among sensors.

Acknowledgments

This research was funded by NASA grants number NNX11AF19G and NNX08AL93A and by USDA NIFA grant number 2011-32100-06016. The U.S. Landsat project management and staff at the USGS National Center for Earth Resources Observation and Science (EROS), Sioux Falls, South Dakota, are thanked for provision of the Landsat ETM + data used to make the WELD products. The USGS EROS and the USDA Forest Service Remote Sensing Application Center (RSAC) are thanked for the provision of the Monitoring Trends in Burn Severity (MTBS) project data. The authors gratefully acknowledge the contribution by Andrea Baraldi,

for providing the spectral rule preliminary classification software and his original implementation of the two pass connected component segmentation algorithm, and for his comments throughout the project and on an original manuscript version.

References

- Arvidson, T., Goward, S.N., Gasch, J., & Williams, D. (2006). Landsat-7 long-term acquisition plan: Development and validation. *Photogrammetric Engineering & Remote Sensing*, 72, 1137–1146.
- Baraldi, A., & Boschetti, L. (2012). Operational automatic remote sensing image understanding systems: Beyond Geographic Object-Based and Object-Oriented Image Analysis (GEOBIA/GEOOIA) – Part 2: Novel system architecture, information/knowledge representation, algorithm design and implementation. *Remote Sensing*, 4(9), 2768–2817.
- Baraldi, A., Durieux, L., Simonetti, D., Conchedda, G., Holecz, F., & Blonda, P. (2010). Automatic spectral-rule-based preliminary classification of radiometrically calibrated SPOT-4/5/IRS, AVHRR/MSG, AATSR, IKONOS/QuickBird/OrbView/GeoEye, and DMC/SPOT-1/2 imagery – Part I: System design and implementation. *IEEE Transactions on Geoscience and Remote Sensing*, 48, 1299–1325.
- Baraldi, A., Puzzolo, V., Blonda, P., Bruzzone, L., & Tarantino, C. (2006). Automatic spectral rule-based preliminary mapping of calibrated Landsat TM and ETM + images. *IEEE Transactions on Geoscience and Remote Sensing*, 44, 2563–2586.
- Barbosa, P.M., Gregoire, J.-M., & Pereira, J.M.C. (1999). An algorithm for extracting burned areas from time series of AVHRR GAC data applied at a continental scale. *Remote Sensing of Environment*, 69, 253–263.
- Bastarrika, A., Chuvieco, E., & Martin, M.P. (2011). Mapping burned areas from Landsat TM/ETM plus data with a two-phase algorithm: Balancing omission and commission errors. *Remote Sensing of Environment*, 115, 1003–1012.
- Boschetti, L., Brivio, P.A., Eva, H.D., Gallego, J., Baraldi, A., & Grégoire, J.M. (2006). A sampling method for the retrospective validation of global burned area products. *IEEE Transactions on Geoscience and Remote Sensing*, 44(7), 1765–1773.
- Boschetti, L., & Roy, D.P. (2009). Strategies for the fusion of satellite fire radiative power with burned area data for fire radiative energy derivation. *Journal of Geophysical Research-Atmospheres*, 114(D20).
- Boschetti, L., Roy, D., & Justice, C. (2009). International global burned area satellite product validation protocol. In CEOS-CalVal (Ed.), *Part I—Production and standardization of validation reference data* (pp. 1–11). USA: Committee on Earth Observation Satellites.
- Boschetti, L., Roy, D., Justice, C., & Giglio, L. (2010). Global assessment of the temporal reporting accuracy and precision of the MODIS burned area product. *International Journal of Wildland Fire*, 19(6), 705–709.
- Chuvieco, E., & Congalton, R.G. (1988). Mapping and inventory of forest fires from digital processing of TM data. *Geocarto International*, 3(4), 41–53.
- Chuvieco, E., Martín, M.P., & Palacios, A. (2002). Assessment of different spectral indices in the red-near-infrared spectral domain for burned land discrimination. *International Journal of Remote Sensing*, 23, 5103–5110.
- Chuvieco, E., Sandow, C., Guenther, K., González-Alonso, F., Pereira, J., Pérez, O., et al. (2012). Global burned area mapping from european satellites: the ESA fire_cci project. *Advances in Remote Sensing and GIS applications in Forest Fire Management From local to global assessments*. (pp. 237).
- Cohen, W.B., Yang, Z., & Kennedy, R. (2010). Detecting trends in forest disturbance and recovery using yearly Landsat time series: 2. TimeSync—Tools for calibration and validation. *Remote Sensing of Environment*, 114, 2911–2924.
- Csiszar, I., Schroeder, W., Giglio, L., Ellicott, E., Vadrevu, K.P., Justice, C.O., et al. (2014). Active fires from the Suomi NPP Visible Infrared Imaging Radiometer Suite: Product status and first evaluation results. *Journal of Geophysical Research, [Atmospheres]*, 119, 803–816.
- Disney, M.I., Lewis, P., Gomez-Dans, J., Roy, D.P., Wooster, M., & Lajas, D. (2011). 3D radiative transfer modelling of fire impacts on a two-layer savanna system. *Remote Sensing of Environment*, 115, 1866–1881.
- Drusch, M., Del Bello, U., Carlier, S., Colin, O., Fernandez, V., Gascon, F., et al. (2012). Sentinel-2: ESA's optical high-resolution mission for GMES operational services. *Remote Sensing of Environment*, 120, 25–36.
- Eidenshink, J., Schwind, B., Brewer, K., Zhu, Z., Quayle, B., & Howard, S. (2007). A project for monitoring trends in burn severity. *Fire Ecology*, 3, 3–21.
- Fraser, R.H., Li, Z., & Cihlar, J. (2000). Hotspot and NDVI differencing synergy (HANDS): A new technique for burned area mapping over boreal forest. *Remote Sensing of Environment*, 74, 362–376.
- Fraser, R.H., Li, Z., & Landry, R. (2000). Spot vegetation for characterizing boreal forest fires. *International Journal of Remote Sensing*, 21(18), 3525–3532.
- García-Haro, F.J., Gilabert, M.A., & Meliá, J. (2001). Monitoring fire-affected areas using Thematic Mapper data. *International Journal of Remote Sensing*, 22, 533–549.
- George, C., Rowland, C., Gerard, F., & Balzter, H. (2006). Retrospective mapping of burnt areas in Central Siberia using a modification of the normalized difference water index. *Remote Sensing of Environment*, 104, 346–359.
- Giglio, L. (2007). Characterization of the tropical diurnal fire cycle using VIRS and MODIS observations. *Remote Sensing of Environment*, 108, 407–421.
- Giglio, L., Descloitres, J., Justice, C.O., & Kaufman, Y.J. (2003). An enhanced contextual fire detection algorithm for MODIS. *Remote Sensing of Environment*, 87, 273–282.
- Giglio, L., Loboda, T., Roy, D.P., Quayle, B., & Justice, C.O. (2009). An active-fire based burned area mapping algorithm for the MODIS sensor. *Remote Sensing of Environment*, 113, 408–420.
- Giglio, L., van der Werf, G.R., Randerson, J.T., Collatz, G.J., & Kasibhatla, P. (2006). Global estimation of burned area using MODIS active fire observations. *Atmospheric Chemistry and Physics*, 6, 957–974.
- Gitas, I.Z., Mitri, G.H., & Ventura, G. (2004). Object-based image classification for burned area mapping of Creus Cape, Spain, using NOAA-AVHRR imagery. *Remote Sensing of Environment*, 92, 409–413.
- GOFC-GOLD (2014). Reducing greenhouse gas emissions from deforestation and degradation in developing countries: A sourcebook of methods and procedures for monitoring measuring and reporting. *GOFC-GOLD Report version COP19-2*. The Netherlands: GOFC-GOLD Land Cover Project Office, Wageningen University (Retrieved from: <http://www.gofcgold.wur.nl/redd/>).
- Goodwin, N.R., & Collett, L.J. (2014). Development of an automated method for mapping fire history captured in Landsat TM and ETM + time series across Queensland, Australia. *Remote Sensing of Environment*, 148, 206–221.
- Griffith, G.E., & Omernik, J.M. (2009). Ecoregions of the United States – Level III (EPA). In C.J. Cleveland (Ed.), *Encyclopedia of earth*. Washington DC: Environmental Information Coalition, National Council for Science and the Environment.
- Hall, D.K., Brown, J., & Johnson, L. (1978). The 1977 tundra fire in the Kokolik River area of Alaska. *Arctic*, 31, 54–58.
- Hall, D.K., Ormsby, J.P., Johnson, L., & Brown, J. (1980). Landsat digital analysis of the initial recovery of burned tundra at Kokolik river, Alaska. *Remote Sensing of Environment*, 10, 263–272.
- Hansen, M.C., & Loveland, T.R. (2012). A review of large area monitoring of land cover change using Landsat data. *Remote Sensing of Environment*, 122, 66–74.
- Hansen, M.C., Potapov, P.V., Moore, R., Hancher, M., Turubanova, S.A., Tyukavina, A., et al. (2013). High-resolution global maps of 21st-century forest cover change. *Science*, 342, 850–853.
- Hanson, S., & Chuvieco, E. (2011). Evaluation of different topographic correction methods for Landsat imagery. *International Journal of Applied Earth Observation and Geoinformation*, 13(5), 691–700.
- Hanson, S., Padilla, M., Corti, D., & Chuvieco, E. (2013). Strengths and weaknesses of MODIS hotspots to characterize global fire occurrence. *Remote Sensing of Environment*, 131, 152–159.
- Harma, K., & Morrison, P. (2003). *Analysis of vegetation mortality and prior landscape condition, 2002 Biscuit Fire Complex*. Winthrop, WA: Pacific Biodiversity Institute.
- Hay, G.J., & Castilla, G. (2008). Geographic object-based image analysis (GEOBIA): A new name for a new discipline? In T. Blaschke, S. Lang, & G.J. Hay (Eds.), *Object-based image analysis – Spatial concepts for knowledge-driven remote sensing applications* (pp. 81–92). Springer-Verlag (Chapter 1.4).
- Henry, M.C. (2008). Comparison of single- and multi-date landsat data for mapping wildfire scars in Ocala National Forest, Florida. *Photogrammetric Engineering and Remote Sensing*, 74, 881–891.
- Henry, M.C., & Yool, S.R. (2002). Characterizing fire-related spatial patterns in the Arizona Sky Islands using Landsat TM data. *Photogrammetric Engineering and Remote Sensing*, 68, 1011–1019.
- Homer, C., Huang, C.Q., Yang, L.M., Wylie, B., & Coan, M. (2004). Development of a 2001 national land-cover database for the United States. *Photogrammetric Engineering and Remote Sensing*, 70, 829–840.
- Houghton, R., Hackler, J., & Lawrence, K. (1999). The US carbon budget: Contributions from land-use change. *Science*, 285, 574–578.
- Huang, C.Q., Coward, S.N., Masek, J.G., Thomas, N., Zhu, Z.L., & Vogelmann, J.E. (2010). An automated approach for reconstructing recent forest disturbance history using dense Landsat time series stacks. *Remote Sensing of Environment*, 114, 183–198.
- Hyer, E., & Reid, J. (2009). Baseline uncertainties in biomass burning emission models resulting from spatial error in satellite active fire location data. *Geophysical Research Letters*, 36, L05802.
- Jin, Y., & Roy, D.P. (2005). Fire-induced albedo change and its radiative forcing at the surface in northern Australia. *Geophysical Research Letters*, 32, L13401.
- Ju, J.C., & Roy, D.P. (2008). The availability of cloud-free Landsat ETM plus data over the conterminous United States and globally. *Remote Sensing of Environment*, 112, 1196–1211.
- Justice, C.O., Csiszar, I., Boschetti, L., Korontzi, S., Schroeder, W., Giglio, L., et al. (2013). Satellite monitoring and inventory of global vegetation fires. In J.G. Goldammer (Ed.), *Vegetation fires and global change – Challenges for concerted international action. A White Paper directed to the United Nations and International Organizations, A publication of the Global Fire Monitoring Center (GFMC)*. Kessel Publishing House.
- Justice, C.O., Smith, R., Gill, A.M., & Csiszar, I. (2003). A review of current space-based fire monitoring in Australia and the GOFC/GOLD program for international coordination. *International Journal of Wildland Fire*, 12, 247–258.
- Justice, C., Townshend, J., Vermote, E., Masuoka, E., Wolfe, R., Saleous, N., et al. (2002). An overview of MODIS Land data processing and product status. *Remote Sensing of Environment*, 83, 3–15.
- Kennedy, R.E., Yang, Z., & Cohen, W.B. (2010). Detecting trends in forest disturbance and recovery using yearly Landsat time series: 1. LandTrendr—Temporal segmentation algorithms. *Remote Sensing of Environment*, 114, 2897–2910.
- Kennedy, R.E., Yang, Z., Cohen, W.B., Pfaff, E., Braaten, J., & Nelson, P. (2012). Spatial and temporal patterns of forest disturbance and regrowth within the area of the Northwest Forest Plan. *Remote Sensing of Environment*, 122, 117–133.
- Kokaly, R.F., Rockwell, B.W., Haire, S.L., & King, T.V. (2007). Characterization of post-fire surface cover, soils, and burn severity at the Cerro Grande Fire, New Mexico, using hyperspectral and multispectral remote sensing. *Remote Sensing of Environment*, 106, 305–325.
- Koutsias, N., & Karteris, M. (2000). Burned area mapping using logistic regression modeling of a single post-fire Landsat-5 Thematic Mapper image. *International Journal of Remote Sensing*, 21, 673–687.

- Kovalskyy, V., & Roy, D.P. (2013). The global availability of Landsat 5 TM and Landsat 7 ETM + land surface observations and implications for global 30 m Landsat data product generation. *Remote Sensing of Environment*, 130, 280–293.
- Lee, D.S., Storey, J.C., Choate, M.J., & Hayes, R. (2004). Four years of Landsat-7 on-orbit geometric calibration and performance. *IEEE Transactions on Geoscience and Remote Sensing*, 42, 2786–2795.
- Lentile, L.B., Holden, Z.A., Smith, A.M.S., Falkowski, M.J., Hudak, A.T., Morgan, P., et al. (2006). Remote sensing techniques to assess active fire characteristics and post-fire effects. *International Journal of Wildland Fire*, 15, 319–345.
- Lhermitte, S., Verbesselt, J., Verstraeten, W.W., Veraverbeke, S., & Coppin, P. (2011). Assessing intra-annual vegetation regrowth after fire using the pixel based regeneration index. *ISPRS Journal of Photogrammetry and Remote Sensing*, 66(1), 17–27. <http://dx.doi.org/10.1016/j.isprsjprs.2010.08.000>.
- Lin, H.W., McCarty, J.L., Wang, D., Rogers, B.M., Morton, D.C., Collatz, G.J., et al. (2014). Management and climate contributions to satellite-derived active fire trends in the contiguous United States. *Journal of Geophysical Research, Biogeosciences*, 119. <http://dx.doi.org/10.1002/2013JG002382>.
- Linn, R.R., & Cunningham, P. (2005). Numerical simulations of grass fires using a coupled atmosphere–fire model: Basic fire behavior and dependence on wind speed. *Journal of Geophysical Research: Atmospheres (1984–2012)*, 110.
- Linn, R., Winterkamp, J., Edminster, C., Colman, J.J., & Smith, W.S. (2007). Coupled influences of topography and wind on wildland fire behaviour. *International Journal of Wildland Fire*, 16, 183–195.
- Liu, Y. (2004). Variability of wildland fire emissions across the contiguous United States. *Atmospheric Environment*, 38, 3489–3499.
- Loboda, T., O'Neal, K.J., & Csizsar, I. (2007). Regionally adaptable dNBR-based algorithm for burned area mapping from MODIS data. *Remote Sensing of Environment*, 109, 429–442.
- López García, M.J., & Caselles, V. (1991). Mapping burns and natural reforestation using thematic mapper data. *Geocarto International*, 1, 31–37.
- Maggi, M., & Stroppiana, D. (2002). Advantages and drawbacks of NOAA-AVHRR and SPOT-VGT for burnt area mapping in a tropical savanna ecosystem. *Canadian Journal of Remote Sensing*, 28(2), 231–245.
- Mallinis, G., & Koutsias, N. (2012). Comparing ten classification methods for burned area mapping in a Mediterranean environment using Landsat TM satellite data. *International Journal of Remote Sensing*, 33(14), 4408–4433.
- Markham, B.L., Storey, J.C., Williams, D.L., & Irons, J.R. (2004). Landsat sensor performance: History and current status. *IEEE Transactions on Geoscience and Remote Sensing*, 42, 2691–2694.
- Masek, J.G., Goward, S.N., Kennedy, R.E., Cohen, W.B., Moisen, G.G., Schleeweis, K., et al. (2013). United States forest disturbance trends observed using Landsat time series. *Ecosystems*, 16, 1087–1104.
- Masek, J.G., Vermote, E.F., Saleous, N.E., Wolfe, R., Hall, F.G., Huemmrich, K.F., et al. (2006). A Landsat surface reflectance dataset for North America, 1990–2000. *IEEE Transactions on Geoscience and Remote Sensing Letters*, 3(1), 68–72.
- Masuoka, E., Roy, D.P., Wolfe, R., Morisette, J., Teague, M., Saleous, N., et al. (2010). MODIS land data products: Generation, quality assurance and validation. In B. Ramachandran, C.O. Justice, & M. Abrams (Eds.), *Land Remote Sensing and Global Environmental Change: NASA's EOS and the Science of ASTER and MODIS* (pp. 511–533). New York: Springer Verlag.
- Meigs, G.W., Kennedy, R.E., & Cohen, W.B. (2011). A Landsat time series approach to characterize bark beetle and defoliator impacts on tree mortality and surface fuels in conifer forests. *Remote Sensing of Environment*, 115, 3707–3718.
- Mouillet, F., Schultz, M.G., Yue, C., Cadule, P., Tansey, K., Ciais, P., et al. (2014). Ten years of global burned area products from spaceborne remote sensing—A review: Analysis of user needs and recommendations for future developments. *International Journal of Applied Earth Observation and Geoinformation*, 26, 64–79.
- Murphy, R.E., Ardanuy, P., Deluccia, F.J., Clement, J.E., & Schueler, C.F. (2006). The visible infrared imaging radiometer suite. *Earth science satellite remote sensing* (pp. 199–223). Berlin Heidelberg: Springer.
- Patterson, M.W., & Yool, S.R. (1998). Mapping fire-induced vegetation mortality using Landsat thematic mapper data: A comparison of linear transformation techniques. *Remote Sensing of Environment*, 65, 132–142.
- Pereira, J.M.C., Chuvieco, E., Beaudoin, A., & Desbois, N. (1997). Remote sensing of burned areas: a review. In E. Chuvieco (Ed.), *A review of remote sensing methods for the study of large wildland fires – Megafires project ENV-CT96-0256* (pp. 127–185). University of Alcalá.
- Pereira, M.C., & Setzer, A.W. (1993). Spectral characteristics of fire scars in Landsat-5 TM images of Amazonia. *International Journal of Remote Sensing*, 14, 2061–2078.
- Pu, R., & Gong, P. (2004). Determination of burnt scars using logistic regression and neural network techniques from a single post-fire Landsat-7 ETM + image. *Photogrammetric Engineering and Remote Sensing*, 70, 841–850.
- Pu, R., Gong, P., Li, Z., & Scarborough, J. (2004). A dynamic algorithm for wildfire mapping with NOAA/AVHRR data. *International Journal of Wildland Fire*, 13, 275–285.
- Randerson, J.T., Chen, Y., van der Werf, G.R., Rogers, B.M., & Morton, D.C. (2012). Global burned area and biomass burning emissions from small fires. *Journal of Geophysical Research – Biogeosciences*, 117. <http://dx.doi.org/10.1029/2012JG002128>.
- Roberts, G.J., & Wooster, M.J. (2008). Fire detection and fire characterization over Africa using Meteosat SEVIRI. *IEEE Transactions on Geoscience and Remote Sensing*, 46, 1200–1218. <http://dx.doi.org/10.1109/Tgrs.2008.915751>.
- Rollins, M.G. (2009). LANDFIRE: A nationally consistent vegetation, wildland fire, and fuel assessment. *International Journal of Wildland Fire*, 18, 235–249.
- Roy, D.P., & Boschetti, L. (2009). Southern Africa validation of the MODIS, L3JRC, and GlobCarbon burned-area products. *IEEE Transactions on Geoscience and Remote Sensing*, 47, 1032–1044.
- Roy, D.P., Boschetti, L., Justice, C.O., & Ju, J. (2008). The collection 5 MODIS burned area product — Global evaluation by comparison with the MODIS active fire product. *Remote Sensing of Environment*, 112, 3690–3707.
- Roy, D.P., Boschetti, L., & Smith, A.M.S. (2013). Satellite remote sensing of fires, chapter 5. In C.M. Belcher, & G. Rein (Eds.), *Fire phenomena and the earth system: An interdisciplinary guide to fire science*. Chichester, England: John Wiley & Sons, Ltd. <http://dx.doi.org/10.1002/978118529539.ch5>.
- Roy, D.P., Frost, P., Justice, C., Landmann, T., Le Roux, J., Gumbo, K., et al. (2005). The Southern Africa Fire Network (SAFNet) regional burned area product validation protocol. *International Journal of Remote Sensing*, 26, 4265–4292.
- Roy, D.P., Giglio, L., Kendall, J.D., & Justice, C.O. (1999). Multi-temporal active-fire based burn scar detection algorithm. *International Journal of Remote Sensing*, 20, 1031–1038.
- Roy, D.P., Jin, Y., Lewis, P.E., & Justice, C.O. (2005). Prototyping a global algorithm for systematic fire-affected area mapping using MODIS time series data. *Remote Sensing of Environment*, 97, 137–162.
- Roy, D.P., Ju, J.C., Kline, K., Scaramuzza, P.L., Kovalskyy, V., Hansen, M., et al. (2010). Web-enabled Landsat Data (WELD): Landsat ETM plus composited mosaics of the conterminous United States. *Remote Sensing of Environment*, 114, 35–49.
- Roy, D.P., & Landmann, T. (2005). Characterizing the surface heterogeneity of fire effects using multi-temporal reflective wavelength data. *International Journal of Remote Sensing*, 26, 4197–4218.
- Roy, D.P., Wulder, M.A., Loveland, T.R., Woodcock, C.E., Allen, R.G., Anderson, M.C., et al. (2014). Landsat-8: Science and product vision for terrestrial global change research. *Remote Sensing of Environment*, 145, 154–172.
- Sa, A.C.L., Pereira, J.M.C., Vasconcelos, M.J.P., Silva, J.M.N., Ribeiro, N., & Awasse, A. (2003). Assessing the feasibility of sub-pixel burned area mapping in miombo woodlands of northern Mozambique using MODIS imagery. *International Journal of Remote Sensing*, 24(8), 1783–1796.
- Schmidt, C.J., Hoffman, J., Prins, E., & Lindstrom, S. (2010). GOES-R advanced baseline imager algorithm theoretical basis document for fire/hot spot characterization, version 2. retrieved from <http://www.goes-r.gov/products/ATBDs/baseline/base-line-fire-hot-spot-v2.0.pdf>
- Schroeder, W., Prins, E., Giglio, L., Csizsar, I., Schmidt, C., Morissette, J., et al. (2008). Validation of GOES and MODIS active fire detection products using ASTER and ETM plus data. *Remote Sensing of Environment*, 112, 2711–2726.
- Schroeder, W., Oliva, P., Giglio, L., Csizsar, I., A. (2014). The new VIIRS 375m active fire detection data product: Algorithm description and initial assessment. *Remote Sensing of Environment*, 143, 85–96.
- Silva, J., Sá, A., & Pereira, J.M.C. (2005). Comparison of burned area estimation derived from SPOT-VEGETATION and Landsat ETM + data in Africa: Influence of spatial pattern and vegetation type. *Remote Sensing of Environment*, 96, 188–201.
- Smith, A.M.S., Drake, N.A., Wooster, M.J., Hudak, A.T., Holden, Z.A., & Gibbons, C.J. (2007). Production of Landsat ETM + reference imagery of burned areas within Southern African Savannahs: Comparison of methods and application to MODIS. *International Journal of Remote Sensing*, 28(12), 2753–2775.
- Smith, A.M.S., & Wooster, M.J. (2005). Remote classification of head and backfire types from MODIS fire radiative power and smoke plume observations. *International Journal of Wildland Fire*, 14, 249–254.
- Sonka, M., Hlavac, V., & Boyle, R. (2008). *Image processing, analysis, and machine vision*, Vol. 3, Toronto: Thomson.
- Sparks, A.M., Boschetti, L., Tinkham, W.T., Smith, A.M.S., & Lannom, K.O. (2015). An accuracy assessment of the MTBS burned area product for shrub-steppe fires in the northern Great Basin, United States. *International Journal of Wildland Fire*, 24, 70–78.
- Stroppiana, D., Bordogna, G., Boschetti, M., Carrara, P., Boschetti, L., & Brivio, P.A. (2012). Positive and negative information for assessing and revising scores of burn evidence. *IEEE Geoscience and Remote Sensing Letters*, 9, 363–367.
- Stroppiana, D., Bordogna, G., Carrara, P., Boschetti, M., Boschetti, L., & Brivio, P.A. (2012). A method for extracting burned areas from Landsat TM/ETM + images by soft aggregation of multiple spectral indices and a region growing algorithm. *ISPRS Journal of Photogrammetry and Remote Sensing*, 69, 88–102.
- Tanre, D., Herman, M., & Deschamps, P.Y. (1981). Influence of the background contribution upon space measurements of ground reflectance. *Applied Optics*, 20(20), 3676–3684.
- Tansey, K., Grégoire, J.M., Defourny, P., Leigh, R., Pekel, J.F., van Bogaert, E., et al. (2008). A new, global, multi-annual (2000–2007) burnt area product at 1 km resolution. *Geophysical Research Letters*, 35. <http://dx.doi.org/10.1029/2007GL031567>.
- Tansey, K., Gregoire, J.M., Stroppiana, D., Sousa, A., Silva, J., Pereira, J.M.C., et al. (2004). Vegetation burning in the year 2000: Global burned area estimates from SPOT VEGETATION data. *Journal of Geophysical Research-Atmospheres*, 109. <http://dx.doi.org/10.1029/2003JD003598>.
- Trigg, S., & Flasse, S. (2000). Characterizing the spectral-temporal response of burned savannah using in situ spectroradiometry and infrared thermometry. *International Journal of Remote Sensing*, 21(16), 3161–3168.
- Trigg, S.N., & Roy, D.P. (2007). A focus group study of factors that promote and constrain the use of satellite-derived fire products by resource managers in southern Africa. *Journal of Environmental Management*, 82, 95–110.
- Trigg, S.N., Roy, D.P., & Flasse, S.P. (2005). An in situ study of the effects of surface anisotropy on the remote sensing of burned savannah. *International Journal of Remote Sensing*, 26, 4869–4876.
- Tyc, G., Tulip, J., Schulter, D., Krischke, M., & Oxford, M. (2005). The RapidEye mission design. *Acta Astronautica*, 56(1), 213–219.
- van der Werf, G.R., Randerson, J.T., Giglio, L., Collatz, G.J., Mu, M., Kasibhatla, P.S., et al. (2010). Global fire emissions and the contribution of deforestation, savanna, forest, agricultural, and peat fires (1997–2009). *Atmospheric Chemistry and Physics*, 10, 11707–11735.

- Van Wagendonk, J.W., Root, R.R., & Key, C.H. (2004). Comparison of AVIRIS and Landsat ETM+ detection capabilities for burn severity. *Remote Sensing of Environment*, 92, 397–408.
- Vanonckelen, S., Lhermitte, S., & Van Rompaey, A. (2013). The effect of atmospheric and topographic correction methods on land cover classification accuracy. *International Journal of Applied Earth Observation and Geoinformation*, 24, 9–21.
- Vermote, & Kotchenova (2008). Atmospheric correction for the monitoring of land surfaces. *Journal of Geophysical Research*, 113, D23S90.
- Westerling, A.L., Hidalgo, H.G., Cayan, D.R., & Swetnam, T.W. (2006). Warming and earlier spring increase western US forest wildfire activity. *Science*, 313, 940–943.
- Wiedinmyer, C., & Hurteau, M.D. (2010). Prescribed fire as a means of reducing forest carbon emissions in the western United States. *Environmental Science & Technology*, 44, 1926–1932.
- Wolfe, R.E., Roy, D.P., & Vermote, E. (1998). MODIS land data storage, gridding, and compositing methodology: Level 2 grid. *IEEE Transactions on Geoscience and Remote Sensing*, 36, 1324–1338.
- Wolfe, R., Nishihama, M., Fleig, A., Kuyper, J., Roy, D., Storey, J., et al. (2002). Achieving sub-pixel geolocation accuracy in support of MODIS land science. *Remote Sensing of Environment*, 83, 31–49.
- Woodcock, C.E., Allen, A.A., Anderson, M., Belward, A.S., Bindschadler, R., Cohen, W.B., et al. (2008). Free access to Landsat imagery. *Science*, 320, 1011.
- Wulder, M.A., White, J.C., Alvarez, F., Han, T., Rogan, J., & Hawkes, B. (2009). Characterizing boreal forest wildfire with multi-temporal Landsat and LiDAR data. *Remote Sensing of Environment*, 113, 1540–1555.
- Yamaguchi, Y., Kahle, A.B., Tsu, H., Kawakami, T., & Pniel, M. (1998). Overview of advanced spaceborne thermal emission and reflection radiometer (ASTER). *IEEE Transactions on Geoscience and Remote Sensing*, 36, 1062–1071.
- Zhang, X., Kondragunta, S., & Roy, D.P. (2014). Interannual variation in biomass burning and fire seasonality derived from geostationary satellite data across the contiguous United States from 1995 to 2011. *Journal of Geophysical Research – Biogeosciences*, 119, 1147–1162.
- Zhang, Q.F., Pavlic, G., Chen, W.J., Fraser, R., Leblanc, S., & Cihlar, J. (2005). A semi-automatic segmentation procedure for feature extraction in remotely sensed imagery. *Computers & Geosciences*, 31, 289–296.